Review Article

Surface electrical stimulation of the auditory cortex preserves efferent medial olivocochlear neurons and reduces cochlear traits of age-related hearing loss

V. Fuentes-Santamaría [a], Z. Benítez-Maicán [a], J.C. Alvarado [a], I.S. Fernández del Campo [b], M.C. Gabaldón-Ull [a], M.A. Merchán [b,**], J.M. Juiz [a,c,**,*]

[a] School of Medicine, Universidad de Castilla-La Mancha (UCLM), Campus in Albacete, 02008, Albacete, Spain
[b] Lab. of Auditory Neuroplasticity, Institute for Neuroscience of Castilla y León (INCYL), University of Salamanca, Salamanca, Spain
[c] Hannover Medical School, Dept. of Otolaryngology and Cluster of Excellence "H4all" of the German Research Foundation, DFG, Carl-Neuberg-Str. 1, 30625 Hannover, Germany

ARTICLE INFO

ABSTRACT

The auditory cortex is the source of descending connections providing contextual feedback for auditory signal processing at almost all levels of the lemniscal auditory pathway. Such feedback is essential for cognitive processing. It is likely that corticofugal pathways are degraded with aging, becoming important players in age-related hearing loss and, by extension, in cognitive decline. We are testing the hypothesis that surface, epidural stimulation of the auditory cortex during aging may regulate the activity of corticofugal pathways, resulting in modulation of central and peripheral traits of auditory aging. Increased auditory thresholds during ongoing age-related hearing loss in the rat are attenuated after two weeks of epidural stimulation with direct current applied to the surface of the auditory cortex for two weeks in alternate days (Fernández del Campo et al., 2024). Here we report that the same cortical electrical stimulation protocol induces structural and cytochemical changes in the aging cochlea and auditory brainstem, which may underlie recovery of age-degraded auditory sensitivity. Specifically, we found that in 18 month-old rats after two weeks of cortical electrical stimulation there is, relative to age-matched non-stimulated rats: a) a larger number of choline acetyltransferase immunoreactive neuronal cell body profiles in the ventral nucleus of the trapezoid body, originating the medial olivocochlear system.; b) a reduction of age-related dystrophic changes in the stria vascularis; c) diminished immunoreactivity for the pro-inflammatory cytokine TNFα in the stria vascularis and spiral ligament. d) diminished immunoreactivity for Iba1 and changes in the morphology of Iba1 immunoreactive cells in the lateral wall, suggesting reduced activation of macrophage/microglia; d) Increased immunoreactivity levels for calretinin in spiral ganglion neurons, suggesting excitability modulation by corticofugal stimulation. Altogether, these findings support that non-invasive neuromodulation of the auditory cortex during aging preserves the cochlear efferent system and ameliorates cochlear aging traits, including stria vascularis dystrophy, dysregulated inflammation and altered excitability in primary auditory neurons.

1. Introduction

Age-related hearing loss (ARHL) is manifested by progressively diminished hearing sensitivity starting at the high frequency end of the audible spectrum, along with difficult separation of auditory signals from background noise and limitations in speech discrimination and perception (Patel and McKinnon, 2018; Keithley, 2020). ARHL is a consequence of neurodegeneration linked to aging involving both the peripheral auditory receptor and the central auditory pathways (Guerrieri et al., 2023; Tu and Friedman, 2018) which affects normal processing of auditory information. Neural transduction and processing of incoming acoustic signals rely on the cochlear sensory neuroepithelium and neuronal pathways ascending from the cochlea to the cortex through relay nuclei in the medulla and pons, midbrain, and thalamus.

Such "bottom-up" processing is mirrored by "top-down" modulation through extensive descending pathways, organized in cascading, multi-level feedback circuits from the cortex down to the auditory thalamus and brainstem (Asilador and Llano, 2021; Malmierca and Ryugo, 2011; Schofield, 2010). Mounting evidence supports that such central descending feedback provides neural substrates for predictive coding and signal discrimination during active or difficult listening, essential for cognition and adaptive behavior (Asilador and Llano, 2021; Carbajal and Malmierca, 2018; Elguada and Delano, 2020). In this regard, age-related disruption of pathways descending from the auditory cortex may be a crucial component of hearing degradation during aging (Peelle and Wingfield, 2016).

Descending central auditory modulation originating in the cortex extends down to the cochlea (Terreros and Delano, 2015), as neurons in the superior olivary complex (SOC) in the pons giving origin to the efferent olivocochlear (OC) pathway, receive abundant descending inputs, either directly from the cortex or indirectly through intervening relays at more rostral auditory nuclei (Terreros and Delano, 2015). The OC pathway is the effector branch of a complex reflex arc originating from afferent auditory nerve fibers which provide indirect, polysynaptic input to efferent OC neurons, comprising the medial and lateral OC systems (MOC and LOC respectively) (reviewed in Lopez-Poveda 2018). MOC neuronal cell bodies are located closer to the midline in the SOC, in the ventral nucleus of the trapezoid body (VNTB), whereas LOC neuronal cell bodies are localized more laterally, in and around the lateral superior olive (Vetter et al., 1991; White and Warr, 1983). MOC axons travel either to the contralateral cochlea, the majority, or to the ipsilateral one, joining the auditory nerve. They end mostly at the base of outer hair cells (OHCs) establishing unique cholinergic synapses (Elgoyhen and Katz, 2012). Activation of MOC neurons by incoming sound results in acetylcholine (Ach) being released from their synaptic endings, modulating contractility of OHCs. This results in reduced active amplification of the mechanical vibrations of the basilar membrane, so that dynamic ranges are extended, and signal detection may be enhanced (Liberman and Liberman, 2019). The contribution of the MOC system, as it pertains to degraded speech recognition in noise and aging is controversial (Abdala et al., 2014; Gafoor and Uppunda, 2023; Kawase and Liberman, 1993; Marrufo-Pérez et al., 2018). However, enhancing MOC synaptic nicotinic Ach receptor (nAchR) machinery by overexpressing nAchR α9 subunit in genetically modified mice, preserves cochlear structure and function from aging (Boero et al., 2020).

Also, interrupting efferent feedback accelerates traits of ARHL in the mouse cochlea (Liberman et al., 2014), although mechanisms are unclear (Lauer, 2017). As far as the LOC system is concerned, neurons project their axons preferentially to the ipsilateral cochlea, where they make multiple synapses with the peripheral processes of spiral ganglion (SG) type I neurons, underneath inner hair cells (IHCs) (Hua et al., 2021). LOC synaptic endings are heterogeneous in neurotransmitter content, which includes Ach and dopamine, in combination with neuroactive peptides and gamma-aminobutyric acid (Altschuler et al., 1986; Gil-Loyzaga, 1995; Ruel et al., 2007). LOC system functions are less worked out, although it may directly regulate the activity of SG type I neurons (Fuchs and Lauer, 2019, Le Prell et al., 2003). Such excitability regulation may contribute to protect SG neurons from noise overstimulation and to balance output from both ears for accurate sound localization (Liberman and Liberman, 2019). Both MOC and LOC protect the auditory receptor from noise overstimulation, and their activity may also provide trophic support to sensory and supporting cells (Liberman and Liberman, 2019; Lauer, 2017). As previously mentioned, integrity of the OC pathway seems necessary for long-term maintenance of cochlear function (Liberman et al., 2014). It has been shown that a decrease in the number of OC neurons during aging predominantly affects MOC neurons, which puts focus on the preservation of the MOC system to limit the impact of ARHL (Vicencio-Jimenez et al., 2021).

Therefore, degraded OC input to the cochlea likely is involved in ARHL and neurons in the auditory brainstem giving origin to the OC

pathways may be driven by direct and/or indirect corticofugal inputs (Terreros and Delano, 2015). Based on these two premises, a testable hypothesis is that stimulation of the auditory cortex (AC) during aging may activate corticofugal pathways, ultimately driving OC neurons, which may spread activity down to the cochlea through OC efferent fibers, resulting in measurable preservation effects on traits of ARHL.

It is known that electrical stimulation delivered on the surface of the brain cortex modulates neuronal excitability and ultimately activity of the cortical network circuits (Mosilhy et al., 2022). Application of this cortical neuromodulation principle has already shown beneficial albeit variably successful effects in several neurological and neuropsychiatric disorders, including tinnitus distress (De Ridder et al., 2021; Lefaucheur, 2008). There is evidence that minimally invasive, epidural anodal electrical stimulation of the AC delivered in short sessions over a period of two weeks, limits noise-induced hearing loss in the rat (Díaz et al., 2021). Also, threshold shifts associated with ARHL are significantly reduced, and wave amplitudes and latencies recover at the end of a similar cortical electrical stimulation protocol applied to aged rats for two weeks, as reported in a related paper in this issue (Fernández del Campo et al., 2024 in this issue).

We sought to test whether surface electrical stimulation of the AC during aging induces changes in auditory brainstem neurons in the SOC giving origin to the medial olivocochlear efferent system, as well as in the aging cochlea. Such changes may unravel foundations of the observed recovery of age-degraded hearing sensitivity induced by cortical electrical stimulation (Fernández del Campo et al., 2024, in this issue). We have used changes in choline acetyltransferase (ChAT) immunolabeling patterns in MOC neurons in VNTB to assess effects of cortical electrical stimulation on cochlear efferent circuits during aging. In the aged cochlea, histological evaluation and immunocytochemical markers were used to test effects of cortical stimulation on age-dysregulated inflammation in the lateral wall, including the stria vascularis, affected early during cochlear aging. In addition, possible changes in primary sensory neuron activity induced by cortical electrical stimulation on aged SG neurons was assessed using calretinin immunolabeling as surrogated marker of neuronal excitability. The picture emerging from this combination of markers suggests that descending spread of cortical electrical stimulation recovers age degraded MOC efferent neurons, ultimately reducing cochlear aging traits.

2. Materials and methods

Fourteen male Wistar rats were used. They were 6-month-old at the beginning of the experimental protocol, with weights ranging from 200 to 220 g. Sex uniformity was preferred to reduce sources of variability and choice was made at random. Animal housing, handling and experimental procedures were conducted according to Spanish and EU legal provisions regarding the protection of animals used in scientific experimentation (Royal Decree 53/2013–Law 32/2007, EU Directive 2010/63) and European Union (Directive 2010/63/EU). Experimental protocols were approved by competent governmental authorities, after validation reports from habilitated institutional "ad hoc" ethics committees on animal experimentation at the University of Salamanca (USAL) and the University of Castilla-La Mancha (UCLM) (Permit Number USAL: 2021-685; Permit Number UCLM: PR-2021-12-24).

2.1. Experimental groups, auditory brainstem recordings, electrode implantation and cortical electrical stimulation

Details of the experimental design, including experimental and control groups, auditory brainstem recordings (ABRs) testing, and cortical electrical stimulation procedure can be found in a related paper by Fernández del Campo and coworkers (Fernández del Campo et al., 2024, in this issue). Briefly, starting at six months of age, auditory brainstem recordings (ABRs) were obtained monthly from rats, using click- and pure tones at 4, 8 and 16 kHz. Auditory thresholds obtained at

6 months of age were taken as normal, baseline values in the Wistar rat (Alvarado et al. 2014). As described previously in detail (Alvarado et al., 2014) age-related threshold shifts in the Wistar rat can be detected at 14 months of age. In this study, significant threshold shifts in click and pure tone responses were consistently detectable at 16 months (64 weeks). This age was thus taken as a safe initial reference of ongoing age-related hearing loss (Fernández del Campo et al. 2024, in this issue). Rats were then implanted with the corresponding electrodes for cortical stimulation (see below) and randomly separated into two groups, a control sham-implanted group, with no electrical stimulation (NES group, n=7) and a group receiving cortical electrical stimulation (ES group, n=7). Animals in the NES and ES groups were handled in identical ways, up to the step of electrical stimulation. At the age of 17.5 months, i.e., 70 weeks, animals in the ES group underwent seven, 10-min epidural anodal electric stimulation sessions on alternate days, from 70 to 72 weeks of age (see below). Five days after the last stimulation session, during week 73, designated for convenience as month 18, animals from both groups were euthanized for further histological processing of the auditory brainstem and cochleae, as detailed below.

2.1.1. Click and pure tone auditory brainstem response (ABR) recordings

The procedure is detailed in Fernández del Campo et al. (2024). Briefly, recordings were carried out under gas anesthesia using a real-time signal processing system RZ6 Multi I/O Processor [Tucker-Davis Technologies (TDT), Alachua, Fl, United States]. Click stimuli were 0.1-ms alternating polarity clicks, delivered at 21 clicks/s and in 10 dB SPL ascending steps from 10 to 90 dB SPL. Tonal stimuli were 0.1-ms pure tones of 4, 8 and 16 kHz delivered at 21 tones/s in descending steps of 10 dB SPL from 80 to 10 dB SPL. Acoustic stimulation was carried out in an acoustically isolated chamber, in closed field via a magnetic speaker (MF1 Multi-Field Magnetic Speaker TDT). ABRs were recorded through subcutaneous needle electrodes at the vertex and the two mastoids. The evoked potentials were then amplified and digitized with a Medusa TA16PA preamplifier and a RA4LI head stage (TDT). The final signal was filtered with a 500 Hz high-pass filter and a 3000 Hz low-pass filter. Monoaural ABRs were recorded from the vertex, using the electrode on the mastoid ipsilateral to the stimulated ear as reference, and that in the contralateral mastoid as the ground. ABRs were sequentially recorded in both ears and analyzed separately. Thresholds were calculated using Matlab (© R-2017). They were defined as the minimum sound intensity that evoked a significant voltage change exceeding the mean ± 2 standard deviations of the voltage value of background activity after the first 1.4 ms of recording.

2.1.2. Electrode implantation

After anesthesia with 2.5% isoflurane, animals were placed in a stereotaxic frame. The Paxinos and Watson stereotaxic coordinates (Paxinos and Watson, 2005) were used to locate the AC (IA:4.08mm/ML:4.5mm) on the surface of the left temporal bone. Then, 1-mm holes were drilled in these coordinates, dropping cold saline (4°C) to prevent thermal lesions. A 1-mm silver ball electrode, the anode, was encrusted into the trepanation orifice in the stimulation side, and a 1-mm diameter screw, serving as cathode, was inserted on the contralateral side. An additional ground screw was inserted in the rostral-most area of the skull. The electrode and the screws were glued to the surface of the skull and covered with dental cement.

2.1.3. Cortical stimulation with direct current

An ISU 200 BIP isolation unit controlled by a CS20 stimulator (Cibertec, Madrid, Spain) was used to deliver a 0.1 mA direct current through the epidural bone-attached electrode (anode). The voltage current was monitored for stability during stimulation sessions. Electrical stimulation was applied to awake animals for seven sessions on alternate days with a duration of 10 min per session (for details, see Colmenárez-Raga et al., 2019).

2.2. Immunoperoxidase immunocytochemistry for ChAT in the auditory brainstem

After completing the cortical stimulation protocol, rats in the ES group, along with matched NES controls, were deeply anesthetized with an intraperitoneal injection of 6% sodium pentobarbitone (60 mg/kg bw) and perfused transcardially with 4% paraformaldehyde in 0.1M phosphate buffer (PB). Brains were dissected, post-fixed and serially sectioned in the coronal plane at a thickness of 40 mm with a sliding freezing microtome (HM 430 Sliding, Microm International, Waldorf, Germany). Sections through the superior olivary complex were immunostained for ChAT with a polyclonal antibody obtained in goat against ChAT from human placenta (Merck Millipore #AB144P RRID: AB_2079751).

Free-floating sections were washed in 0.1 M PB, pH 7.6, and endogenous peroxidase activity was inhibited by incubation in 10% methanol + 3% H_2O_2 in 0.1 M PB for 10 min. Sections were washed in PB and 0.05 M Tris-buffered saline, pH 8.0 + Triton X-100, 0.5% (T9284 Sigma, St. Louis, MO, USA; TBS-Tx), after which they were incubated in ChAT antiserum at 1:100 dilution in 0.05 M TBS+0.3%Triton-X (TBS-Tx) for 48 h at 4°C. Nonspecific labeling was blocked using 10% fetal calf serum. After washing three times in TBS-Tx for 15 min, sections were incubated with an anti-goat biotinylated secondary antibody (biotinylated anti-goat IgG H+L, BA-5000; Vector, Burlingame, CA, USA) at 1:200 dilution in TBS-Tx for 120 min at room temperature. Sections were then washed with TBS-Tx and incubated for 180 min in avidin/biotin–peroxidase (ABC complex, Vectastain Standard ABC kit PK-4000; Vector Laboratories,Spain) and further washed with TBS-Tx, followed by Tris HCl, pH 8.0. They were then incubated in 3,3´-diaminobenzidine tetrahydrochloride (DAB; D-9015; Sigma-Aldrich, St. Louis, MO, USA) with 0.006% H_2O_2 to visualize the peroxidase reaction. One section per case was used as a negative control, by processing without the primary antibody to test the specificity of the immunostaining detection system. All incubation steps and development in DAB were carried on paired sections from ES and NES animals, with identical times throughout all the steps of the immunostaining procedure to secure consistent comparison of the immunolabeling signal.

2.3. ChAT immunoreactive neuronal cell body profile counts in the VNTB

Eight serial sections at equivalent interaural levels (from IA -0.12 to IA +0.24) containing VNTB were selected from each animal in the ES and NES groups to allow precise comparison of the number of ChAT positive cell body profiles. Microphotograph mosaic assemblies of the VNTB ipsi- and contralateral to the electrode location were taken at 5X magnification under a Leica DMRX microscope with a MBF camera (MBF Bioscience CX9000; Williston, VT, USA) using the software Neurolucida (NL-Vs 8.0, MicroBrightField®, Inc., Williston, VT, USA).

Immunoreactive neuronal profiles were counted using the "Multipoint" tool in the software ImageJ by two experienced microscopists, blinded to the experimental (ES) or control (NES) conditions. Counts were made separately for the ipsilateral and contralateral VNTB.

2.4. Cochlear histology

Cochleae from rats in the ES and NES groups were also collected after transcardial fixation. They were then postfixed by intra-scalar instillation and further immersion in 4% p-formaldehyde in 0.1 M PB for 48 hours. After extensive washing in PB, cochleae were decalcified in 10% EDTA for 7 days. Once decalcified, they were cryoprotected in 30% sucrose in 0.1 M PB, further embedded in a 10% gelatin solution in the same cryoprotection medium and then stored at -80°C. After temperature equilibration in the cryostat chamber, cochleae were oriented for sectioning in the modiolus plane. Twenty μm-thick sections were obtained in a cryostat and serially mounted onto gelatin-coated slides. Alternate slides were stained with hematoxylin/eosin (H/E) for

conventional photonic microscopy. For H/E, slides were stained in hematoxylin solution (Panreac AppliChem, Barcelona, Spain) for 1 minute, rinsed in distilled water, counterstained in eosin (Merck Life Science S.L. U., Madrid, Spain) for 15 minutes, dehydrated in series of ethanol solutions (50%, 70%, 95%, and 100%; 3 changes, 1 minute each), cleared in xylene and finally cover slipped with Cytoseal (Stephens Scientific, Kalamazoo, MI, USA).

In addition, double fluorescent staining with biotin-phalloidin (Pha) (B7474; 1:100, Thermo Fisher Scientific), incubated for 1h in Alexa Fluor 488 streptavidin (1:100; Thermo Fisher Scientific) and counterstained with antifade mounting medium with DAPI (H-1200-10; Vectashield, Spain) was used for correlative higher resolution microscopy analysis of the stria vascularis, using laser scanning confocal microscopy, as described below.

2.4.1. Morphometry of the stria vascularis

Measurements were performed on H/E-stained mid-modiolar cochlear sections collected 20 μm apart. Four sections from the cochlea ipsi- and contralateral to the stimulated cortical side from each animal in the ES and NES groups were used. A similar procedure has been reported elsewhere (Fuentes-Santamaría et al., 2022; Shin et al., 2019). Images of selected fields (40x magnification) were captured, and the SV thickness measured by using ImageJ software (NIH, Bethesda, MD, United States). The SV of each cochlea was divided into 10 orthogonal measurements along its length. Values were averaged and expressed as mean ±SD.

2.5. Immunofluorescence immunocytochemistry for TNFα and Iba1

Cochlear sections were also processed for double-immunofluorescence labeling for Iba-1 (019-19741; rabbit polyclonal antibody, 1:2000; Wako Pure Chemical Industries, Germany) and TNFα (SC-1351; goat polyclonal antibody, 1:100, Santa Cruz, Biotechnology, Inc. Germany) or Iba-1 and phalloidin. After rinsing in PBS-Tx (0.2%), cochlear sections were blocked for 1 h with 10% bovine serum albumin in PBS-Tx (0.2%), and then incubated overnight in the primary antibodies above-mentioned. The next day, they were rinsed in the same buffer solution and incubated in the corresponding secondary antibodies, either in donkey anti-rabbit conjugated to Alexa Fluor 488 and donkey anti-goat conjugated to Alexa Fluor 594 or in goat anti-rabbit conjugated to Alexa Fluor 594 secondary antibodies (1:100, Thermo Fisher Scientific) for 2 h at room temperature. Immunofluorescent sections stained with Iba1 were subsequently incubated with biotin-phalloidin (Pha) for 2h, rinsed, incubated for 1h in Alexa Fluor 488 conjugated to streptavidin, counterstained with DAPI, cover slipped and stored overnight at 4^0 C, as previously indicated.

Image acquisition was performed with a multichannel laser scanning confocal microscope (LSM 710; Zeiss, Germany) with excitation wavelengths: 405, 488, and 594 nm. For each dye analyzed, thin optical sections (2.5 μm) were acquired under identical offset and gain conditions using a 40x Plan Apo oil-immersion objective (1.4 NA) and stacked to create high-resolution Z-series. Maximum intensity projections of a confocal Z-stack were created using ZEN 2009 Light Edition software (Zeiss).

2.6. Immunoperoxidase immunocytochemistry for calretinin

Fixed cochleae were decalcified and cryosectioned as previously described. Sections were rinsed in phosphate-buffered saline (PBS) containing 0.2% Triton X-100 (Tx) and blocked for 1h at room temperature with 10% bovine serum albumin in PBS-Tx (0.2%). Cochlear sections were then incubated overnight in a humidity box at 4°C with goat anti-calretinin polyclonal primary antibody (7699/3H; 1:1000; Swant, Bellinzona, Switzerland). The next day, after several rinses in PBS-Tx 0.2%, sections were incubated for 2h in biotinylated goat anti-rabbit (1:200, Vector Laboratories, Spain), followed by 1h in avidin-biotin-peroxidase complex solution (ABC) (ABC kit, Vector

Laboratories, Spain). The peroxidase chromogenic substrate 3,3'-diaminobenzidine tetrahydrochloride (DAB) with H_2O_2 was used to visualize the reaction. Finally, sections were rinsed, and cover slipped using Cytoseal. Images were captured using a DXM 1,200 C digital camera (Nikon Instruments Europe B.V., Amsterdam, Netherlands) attached to a Nikon Eclipse 80i photomicroscope (Nikon Instruments Europe B.V., Amsterdam, Netherlands).

2.6.1. Densitometric quantification of calretinin immunolabeling

Procedures are described in detail elsewhere (Alvarado et al., et al., 2016; Fuentes-Santamaria et al., 2005, 2017, 2019). Briefly, captured digital images with gray scale values from 0 to 255 were normalized. A threshold of two standard deviations above the intensity value of the corresponding SG field was set. The mean gray level of calretinin immunostaining in the SG was obtained as a surrogated measure of relative protein content in the control (NES) and experimental (ES) conditions. The percentage of variation of mean gray levels, expressed as a percentage of increase/decrease relative to the control condition was obtained, to facilitate comparisons.

2.7. Statistical tests

To evaluate ChAT immunostaining, statistical analysis was performed using IBM® SPSS® software, version 26.0.0.2 for Mac (IBM Corp. and SPSS Inc., Chicago, IL, United States, RRID: SCR_002865). The F of Friedman non-parametric test was used to assess differences between the number of cells ipsilaterally and contralaterally. . Differences between groups (NES and ES) in the number of ChAT positive cells in the VNTB were determined using the non-parametric U of Mann-Whitney test. Statistical significance was set at $p < 0.05$.

To assess SV thickness and CR immunostaining in the cochlea, comparisons among the different groups were performed using two-way analysis of variance (ANOVA). Electrode insertion with (ES) or without (NES) cortical electrical stimulation was the independent variable and SV thickness and densitometric measures of CR immunostaining were dependent variables. The possible statistically significant main effect of cortical electrical stimulation on each dependent variable was evaluated. If the analysis showed a significant effect or interaction of the variables, a Scheffé post hoc analysis was used for comparisons among groups. Significance levels (α) and power (β) were set to 0.05 and 95%, respectively.

3. Results

3.1. Changes in auditory thresholds after surface electrical stimulation of the auditory cortex in the aged rat

Age-related threshold shifts in the Wistar rat have been described previously (Alvarado et al., 2014). A detailed account of differences in ABR thresholds and wave amplitudes and latencies between ES and NES animal groups can be found in a related paper by Fernández del Campo and coworkers (Fernandez del Campo et al., 2024, in this issue).As shown in Table 1, threshold differences greatly increased between 16 and 18 months of age in the NES group rats, both with clicks, showing

Table 1
Percent changes in ABR thresholds after click and pure tone stimulation in NES and ES animal groups at the end of the intervention protocol. (after data from Fernandez del Campo et al 2024).

% change in threshold	Click	Pure tone 4 kHz	Pure tone 8 kHz	Pure tone 16 kHz
16 months-18 months NES	37.13 %	22.14 %	21.23 %	15.08 %
16 months-18 months ES	12.94 %	0.74 %	5.89 %	0.18 %

threshold increases over 37% at 18 months, relative to threshold values at 16 months, and pure tones, with increases ranging from 15% to 22%, depending on the tone frequency (Table 1). In contrast, anodal electrical stimulation of the AC initiated at the age of 17.5 months, delivered in 10 min sessions on alternate days for two weeks in the ES group, resulted in a large reduction of threshold differences between 16- and 18-month-old animals, relative to the sham-stimulated NES group. Click thresholds still increased between 16 and 18 months in the ES group. However, increases were over three times lower than in the NES group. Such an attenuation of age-related increases in click auditory thresholds was also reflected in pure tone thresholds (Table 1), supporting slowdown of hearing sensitivity loss induced by electrical stimulation of the AC during aging.

3.2. Effects of cortical electrical stimulation on ChAT-immunoreactive MOC neurons in the VNTB of aged rats

Immunoperoxidase immunolabeling for ChAT in brainstem sections showed immunostained neuronal cell bodies and dendrites in the SOC, mainly in LSO and VNTB (Fig. 1A). For the aims of this study, we focused on ChAT immunoreactive neuronal cell bodies located in the VNTB, the main origin of MOC neurons in the SOC (Guinan et al., 1983).

ChAT-immunoreactive neurons in the VNTB are packed between commissural fibers of the trapezoid body (TB) (Fig.1). Cell bodies are medium to small in diameter and their neuronal shape is stellate or fusiform, depending on the orientation of their dendritic fields relative to the fiber fascicles of the TB (Fig. 1A, B). In other words, their intensely
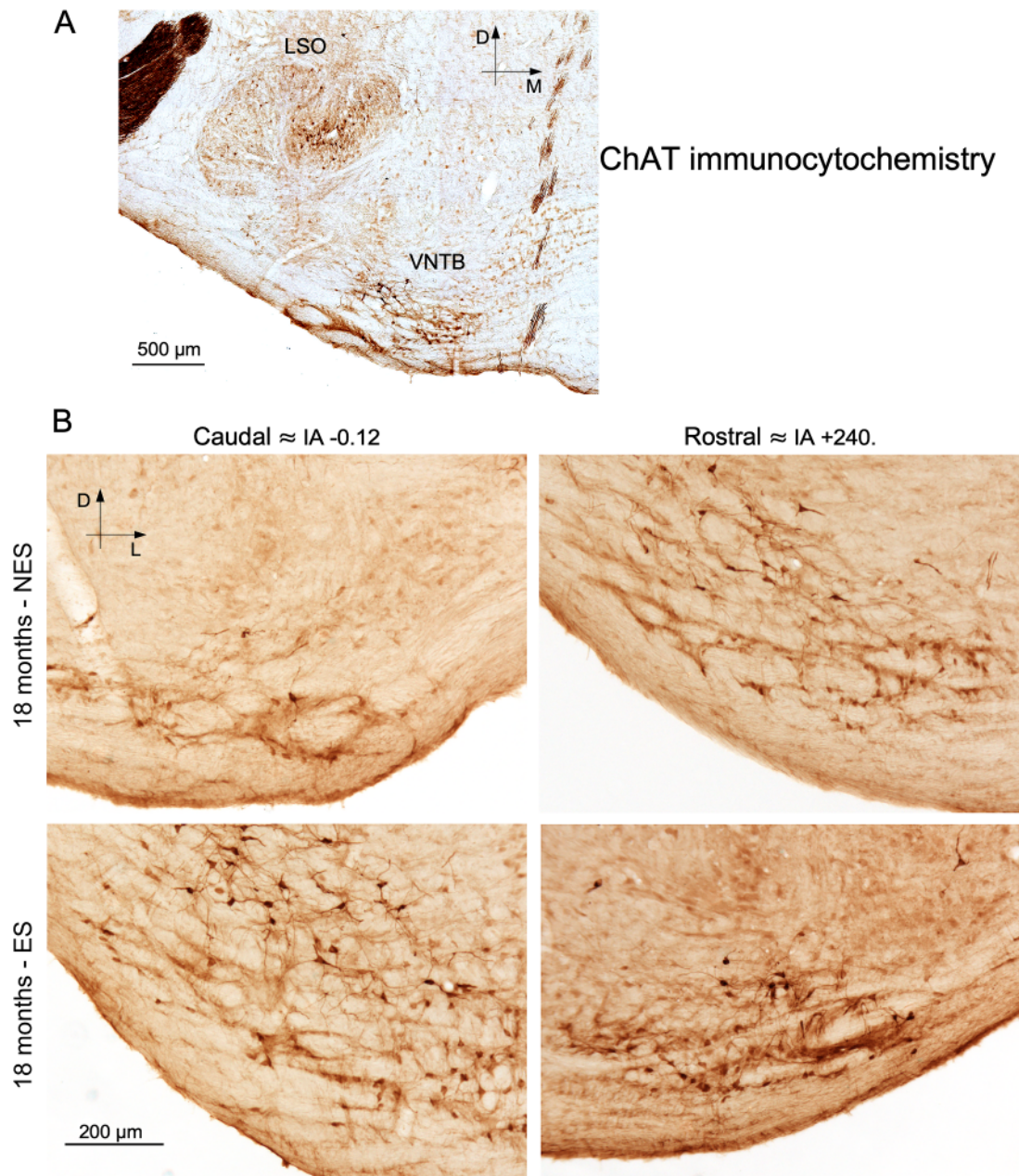

Fig. 1. ChAT immunoreactivity in the superior olivary complex after cortical electrical stimulation during aging
A: Low magnification photomicrograph of a section through the superior olivary complex showing localization of ChAT immunolabeled neurons. Immunoperoxidase immunostaining shows localization of ChAT immunolabeled neurons in the LSO and VNTB. D, dorsal; M, medial. C: Photomicrographs of representative ChAT immunolabeled sections through equivalent caudal and rostral regions of the VNTB from NES and ES animals after completing the electrical stimulation protocol. There are visible differences in the density of ChAT immunoreactive neuronal cell bodies in ES and NES animals. D, dorsal; L, lateral.

immunoreactive dendrites are parallel or orthogonal to the course of the TB (Fig 1). Due to extensive dendritic distribution, qualitative evaluation of ChAT immunoreactive dendrites, along with neuronal cell bodies, among and across the TB fascicles also allows to detect differences between experimental (ES) and control (NES) groups. In this way, by comparing serial sections between both experimental groups at similar rostro-caudal levels, the immunostaining density of immunolabeled neuronal somata, individual dendritic trunks, and dendritic processes packed among TB fascicles appears less intense in the NES animals (Fig. 1B). Counts of ChAT immunoreactive neuronal cell body profiles in the VNTB showed that the NES group had a statistically significant lower number of ChAT-immunoreactive neurons than the ES group after completing the electrical stimulation protocol at 18 months of age. These differences were detected both in the VNTB ipsilateral and contralateral to the position of the stimulation electrode in the AC (Fig. 2). Compared with the NES group, after cortical stimulation in the ES group there were on average 1.3 times more neuronal cell body profiles in the VNTB ipsilateral to the stimulation and 1.2 in the contralateral side (Fig. 2).

3.3. Effects of cortical electrical stimulation on the microscopic structure of the stria vascularis and spiral ganglion in the aging cochlea

Cochlear sections stained with hematoxylin-eosin (H/E) showed better structural preservation of the stria vascularis (SV) in aged rats in the ES group, i.e., after a multisession, two-week cortical electrical stimulation, than in aged, sham-implanted, non-stimulated control rats

Means and SDs

	Ipsilateral	contralateral
NES	588 ± 93	512.8 ± 93
ES	719.8 ± 95.5	648.1 ± 94.8

Fig. 2. Counts of cell body profiles in the VNTB of ES and NES rats
Bar graph with counts of ChAT-immunolabeled cell body profiles in VNTB, showing significantly increased numbers in electrically stimulated (ES) relative to non-stimulated (NES) animals. The F of Friedman non-parametric test was used to assess differences between the number of cells ipsilaterally and contralaterally. Differences between groups (NES and ES) in the number of ChAT positive cells in the VNTB were determined using the non-parametric U of Mann-Whitney test. *p<0.05, **p<0.01.

in the NES group (Fig. 3). In the ES group, both cochleae, ipsi- and contralateral to the stimulation electrode location consistently showed a characteristic layered cellular arrangement of the SV, compared with aged, non-stimulated animals in the NES group in which the normal organization of the SV in marginal, intermediate and basal cell layers was distorted and less distinguishable (Fig. 3A-B, 3F-G and 3K-L). Degenerative/atrophic structural changes in the SV during aging in the Wistar rat have been described previously (Fuentes-Santamaría et al., 2022).

The spiral ligament (SL) underlying the SV frequently appeared partially detached from the adjacent basal cell layer of the SV in aged rats in the NES group, with long, empty gaps between them (arrows in Fig. 3B). However, such detachments were less evident or absent in cochleae from aged rats in the ES group, in which there was little or no intervening discontinuity between the SL and the SV (arrows in Fig.3G and 3L), other than spaces occupied by recognizable small blood vessels. Other areas of the SL, such as the fibrocyte IV/II regions and adjacent root cells did not show differences between the ES and NES cochleae (Fig. 3C, 3H and 3M). As far as SG neurons are concerned, no differences were observable with H/E staining in SG neuronal packing in Rosenthal's canal between aged, electrically stimulated rats in the ES group and NES controls (Fig. 3D, 3I and 3N), although formal quantification was not carried out. In addition, the morphology of SG neurons did not differ between both groups. SG neuron cell bodies with similar structural features, including regular, visible nuclei were easily recognized (arrows in Fig. 3E, 3J and 3O).
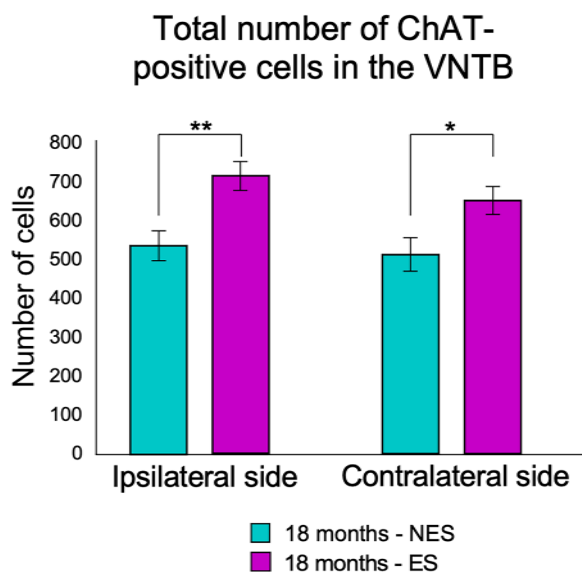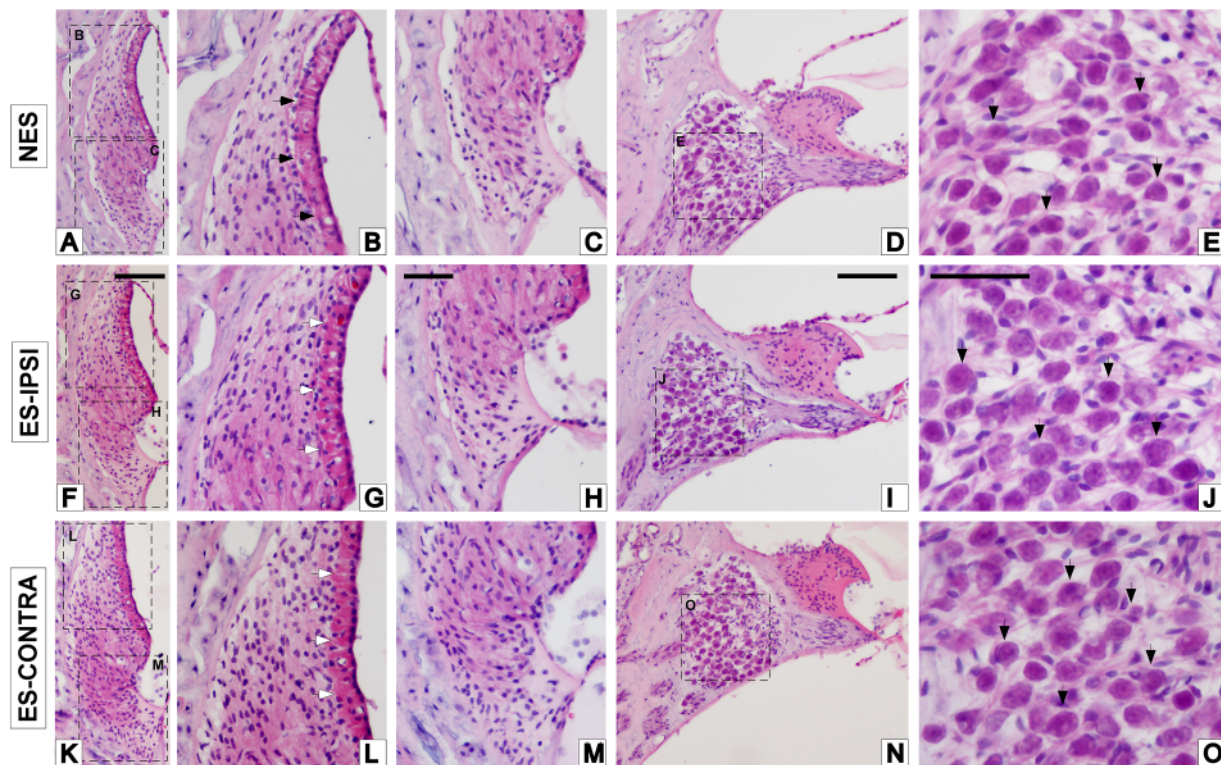
3.3.1. Correlative conventional light microscopy and confocal laser scanning microscopy and morphometry of the stria vascularis

Higher resolution microscopic analysis of the SV, carried out by correlating H/E staining with double fluorescence with DAPI and phalloidin analyzed with laser scanning confocal microscopy, confirmed a comparatively less distorted architecture of the SV in aged rats in the ES group (Fig. 4A-F). In this experimental group, the intermediate and, even more evidently, the basal layer of the SV showed more regularly arranged and packed DAPI-stained nuclei (Fig. 4D, F) in comparison with the SV in aged rats in the NES group (Fig. 4B). Also, in the NES group detachments between the disorganized basal cell layer of the SV and the adjacent SL were more evident than in rats in the ES group, with the higher resolution provided by double fluorescence combined with confocal microscopy (Fig. 4A, C, E). Besides a better-preserved cellular organization, measurement of the thickness of the SV showed that in the ES group the SV was significantly thicker on average (22.45 ±1) than in the NES group (25.66 ±2.81 and 26.24± 1.49; for the SV ipsi- and contralateral to the stimulation sides; respectively) (Fig. 4G).

3.4. Changes in Iba1 and TNFα immunolabeling in the lateral wall of the cochlea after cortical electrical stimulation during aging

Besides degenerative/atrophic changes in the SV and SL, several inflammation-related markers were upregulated during aging in the lateral wall of the cochlea in the rat, including the SV and SL, as previously reported in detail with immunocytochemistry (Fuentes-Santamaría et al., 2022).

The ionized calcium binding adapter protein 1, or Iba1, is a marker of activated macrophage/microglia, an essential component of the inflammatory response. Intense immunofluorescence immunolabeling for Iba1 was seen in the SV and SL of aged rat cochleae in the NES group (Fig. 5A, B, see also Fig. 6B). There were abundant Iba1 immunolabeled cells with thick and short cytoplasmic expansions, giving cells an ameboid appearance (Figs. 5B, 6B). In contrast, in the SV and adjoining SL of aged rats in the ES group, Iba1 immunofluorescence immunolabeling was overall less evident (Fig. 5D-E, 5G-H and Fig. 6B, 6E and 6H). Also, in the ES group immunolabeled macrophage/microglia had regular, more delicate contours with longer and thinner cytoplasmic processes (Fig. 5E, 5H and Fig. 6E, H). Iba1-immunolabeled cellular profiles

Fig. 3. Spiral ligament, stria vascularis and spiral ganglion after electrical stimulation of the auditory cortex during aging.
A, F, K: Hematoxylin/eosin-stained sections of the lateral wall from the cochlea of (A) a representative 18 month-old sham-implanted rat receiving no cortical electrical stimulation (NES) and the same region from a rat of the same age after two weeks of cortical electrical stimulation (F, K), corresponding to the lateral wall of the cochlea ipsi- (ES-IPSI) or contralateral (ES-CONTRA) to the stimulated side. Inserts in A, F and K outlining the stria vascularis and underlying spiral ligament are shown at higher magnification in photomicrographs B, G and L. Inserts in A, F and K outlining the spiral prominence region are shown at higher magnification in photomicrographs C, H and M. **B, G, L:** Higher magnification photomicrographs of the corresponding inserts in A, F and K, showing details of the stria vascularis in NES (B) and ES rats in the cochleae ipsi- (G) and contralateral (L) to the cortical stimulation side. In ES rats, the layered architecture of the stria vascularis is better defined, with more nuclei visibly aligned, particularly in intermediate and basal layers (compare B with G and L). In addition, in ES animals, the basal layer of the stria vascularis shows continuity with the underlying spiral ligament (white arrows in G and L), whereas in NES rats the stria vascularis often appears detached, with elongated empty spaces separating it from the spiral ligament (black arrows in B). **C, H, M:** The region of the spiral prominence shows no visible differences between NES (C) and ES animals (H, M). **D, I, N:** Rosenthal's canal from the same sections. Inserts E, J, O are shown at higher magnification in the corresponding photomicrographs. There are no differences in the packing or distribution of spiral ganglion neuron cell bodies between NES (D) and ES animals, be it in the cochlea ipsilateral (I) or contralateral (N) to the stimulated auditory cortex. **E, J, O:** Higher magnification photomicrographs of the inserts in D-N. Spiral ganglion neuron cell bodies have similar morphologies in NES (E) and ES rats (J, O). Scale bars: 100μm in F; 50μm in H; 100μm in I and 50μm in J.

were also seen in the SG, processes meandering among neuronal cell bodies (Fig. 5C, 5F and 5I). No differences in morphology or distribution of Iba1 immunolabeled cells in the SG were observed between NES (Fig. 5C) and ES rats (Fig 5F, 5I).

Control NES aged rats showed extensive immunolabeling for the early pro-inflammatory cytokine marker TNFα in the SV and SL (Fig. 6A, C). In contrast, in ES rats TNFα immunolabeling in the SV and SL consistently showed comparatively attenuated intensity in both cochleae, ipsi- and contralateral to the stimulation electrode location (Fig. 6F, 6I). Diminished TNFα immunolabeling in the SV and SL of ES rats relative to NES rats, was better visualized in combination with Iba1 immunolabeling. In NES rats, immunolabeling for Iba1 in activated macrophage/microglia frequently co-localized with TNFα (Fig. 6 A-C). This was particularly evident in clearly delineated, co-labeled macrophage/microglia (Fig. 6A) extending thick processes forming a "palisade" lining the border between the SV and underlying SL (Fig. 6A, B). In contrast, in ES rats Iba1 co-localization with TNFα in double immunostaining experiments (Fig. 6D, 6G) was visually less intense than in NES control rats (Fig. 6A).

3.5. Cortical electrical stimulation and calretinin immunolabeling in spiral ganglion neurons during aging

Immunoperoxidase immunostaining with calretinin in cochlear sections, showed differences in immunostaining intensity in SGN cell bodies between aged rats in the ES and NES groups (Fig. 7A-F). Overall, calretinin immunolabeling was clearly more intense in SGN cell bodies after cortical stimulation, in rats from the ES group, both ipsi- and contralateral to the side of electrode placement, as shown in the example of Fig. 7 (C-F), taken from representative sections from middle cochlear turns. As shown in Fig. 8, differences in calretinin immunostaining in SG neuron cell bodies were evident throughout Rosenthal's canal in the basal, middle, and apical turns, with SGN cell bodies in rats in the NES group showing consistently diminished immunolabeling intensity throughout the entire spiral ganglion extension, compared with rats in the ES group (Fig. 8A-I).

Quantification of calretinin immunolabeling intensity confirmed and extended qualitative microscopic observations. Mean gray levels of calretinin immunoreaction product density were significantly increased in SG neuron cell bodies of rats in the ES group, both ipsi- and contralateral to the stimulation electrode placement in the cortex, relative to levels in SG neuron cell bodies of rats in the NES group (Fig. 8J). To facilitate comparisons, the percentage of variation of mean gray levels
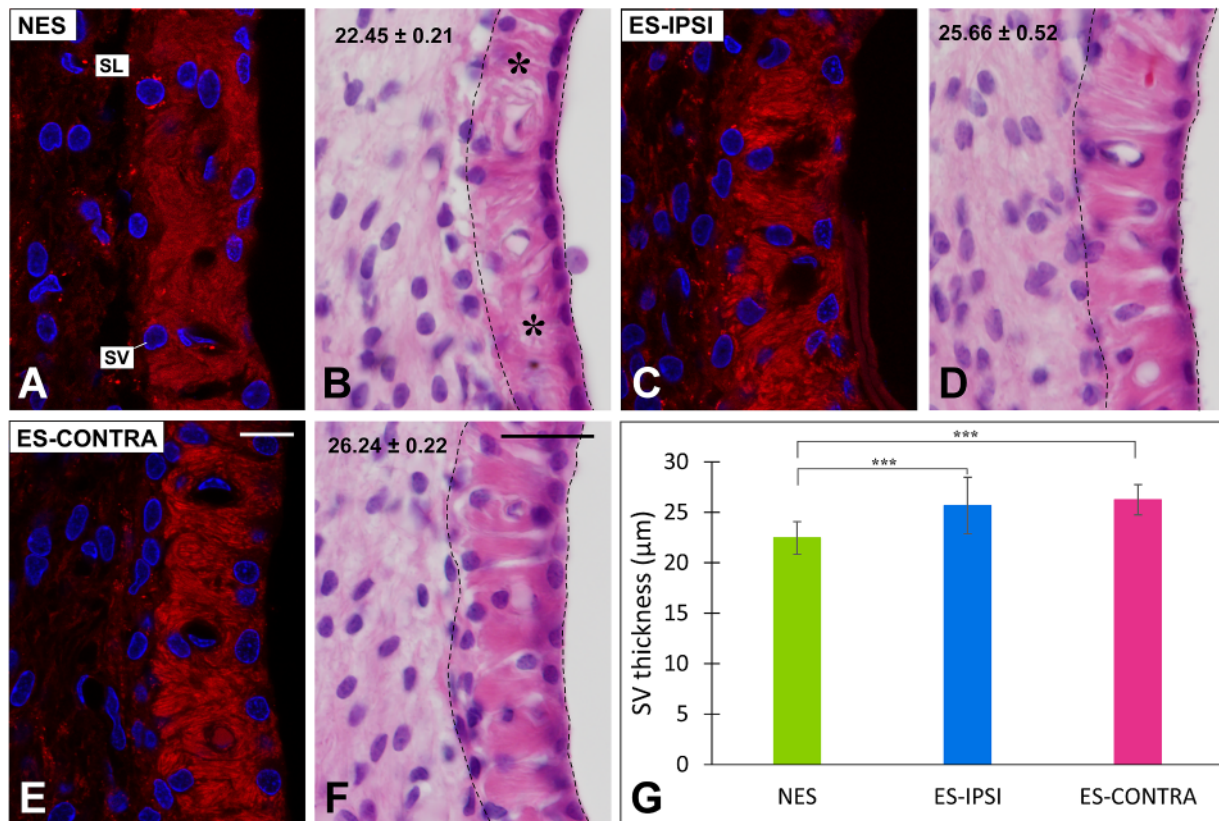
Fig. 4. The stria vascularis after electrical stimulation of the auditory cortex during aging

A, B: Photomicrographs of the stria vascularis from cochlear sections stained with double fluorescence for Phalloidin (red) and DAPI (blue) (A) or hematoxylin/eosin (B) from a sham implanted, non-stimulated (NES) 18-month-old rat. **C, D, E, F:** Photomicrographs of the stria vascularis from cochlear sections stained with double immunofluorescence for Phalloidin (red) and DAPI (blue) (C, E) or hematoxylin/eosin (D,F) from an rat of the same age, after two weeks of cortical electrical stimulation (ES), corresponding respectively to the stria vascularis of the cochlea ipsi- (ES-IPSI) or contralateral (ES-CONTRA) to the electrically stimulated side. In the stria vascularis from the ES rat, intermediate and basal cell layers appear better organized and preserved and cytoplasmic structure and cellular limits are better defined (C-F) than in the NES rat (A, asterisks in B). **G:** Bar graph showing variation in the thickness of the aged stria vascularis after electrical stimulation of the auditory cortex. ES rats show statistically significant increases in the thickness of the stria vascularis relative to NES rats. Comparisons among the different groups were performed using two-way ANOVA ($F_{(2, 128)} = 56.89$) and Scheffé post hoc analysis was used for comparisons among groups. Significance levels (α) and power (β) were set to 0.05 and 95%, respectively, ***$p < 0.001$. Abbreviations: SV, stria vascularis; SL, spiral ligament. Scale bars: 10μm in E; 25μm in F.

for calretinin immunolabeling in the SGN in the ES group is shown in Fig. 8K.

4. Discussion

In this report, we show that surface, epidural electrical stimulation of the auditory cortex (AC) in the aging rat with an extended, two-week, multisession stimulation protocol with DC current (see Fernández del Campo et al., 2024 in this issue) resulted in histological and cytochemical changes suggesting effects on auditory aging in the auditory brainstem and in the cochlea. Gathered evidence supports that such effects on auditory aging may involve spread of electrical stimulation down corticofugal pathways reaching neurons in the VNTB of the SOC, originating the MOC efferent system, ending primarily on cochlear OHCs.

4.1. VNTB: Larger numbers of ChAT-immunoreactive neuronal cell body profiles after cortical electrical stimulation

Firstly, we found that after completing the cortical electrical stimulation protocol, ChAT immunostaining in the VNTB increased in the experimental ES group relative to the control NES group as seen by increased ChAT immunolabeling, with significantly larger numbers of immunolabeled neuronal cell body profiles in VNTB in the ES experimental group. There is evidence in many species including the rat,

supporting that most MOC neuronal cell bodies are localized in the VNTB (White and Warr, 1983) and that they contain ChAT for the synthesis of Ach (Vetter et al., 1991), their main neurotransmitter released at their synaptic contacts on the base of cochlear OHCs (Blanchet et al., 1996). Therefore, changes in ChAT immunolabeling in the VNTB are informative of ongoing changes in the MOC system occurring for instance during aging (Vicencio-Jimenez et al., 2021). In our case, electrical stimulation-elicited neural activity propagating down from the AC to the VNTB, resulted in increased numbers of ChAT immunoreactive cell body profiles in the VNTB of ES aged rats, compared to those in the NES group. Biases in cell body counting were limited by dual blinded counting, thus rendering reliable counting ratios, which are a reasonable approximation to differences between the experimental (ES) and control (NES) groups. . Thus, the number of ChAT immunoreactive neurons in the aged VNTB likely increases after cortical electrical simulation due either to preservation from death, recovery of detectable ChAT levels because of activity-induced increase in protein synthesis (Hyson and Rubel, 1995), or both. The fact that the same rostro-caudal levels of the VNTB were compared in ES and NES animals and that ChAT immunocytochemistry was carried out under identical incubation conditions strengthens this interpretation. In other words, age-related loss of MOC neurons, and corresponding efferent innervation to the cochlea, shown by us and previously reported in other rodents (Radtke-Schuller et al., 2015; Vicencio-Jimenez et al., 2021) may be reversed or slowed down by electrical stimulation of the AC. In this regard, modulation of ChAT
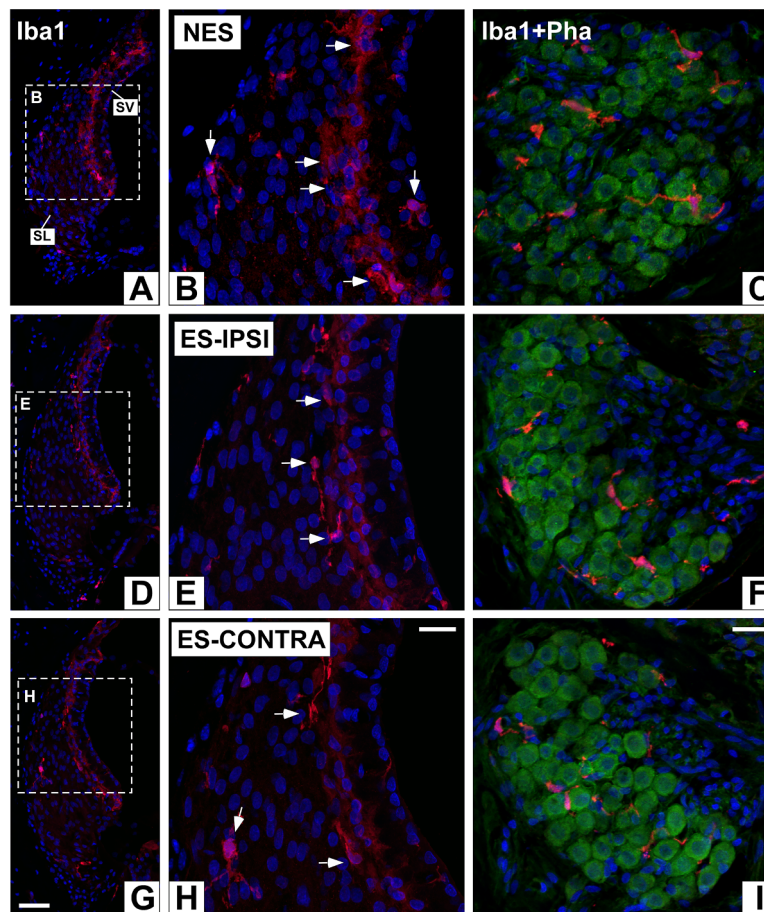
Fig. 5. Iba1 immunolabeling in the cochlear lateral wall and spiral ganglion after cortical electrical stimulation during aging

A, D, G: Low magnification laser scanning confocal photomicrographs showing Iba1 immunolabeling (red) in the lateral wall. Iba1 immunolabeling is concentrated in a band at the border between SV and SL. Immunolabeling density and intensity appear higher in control NES (A) than in the ES rat (D, G). Boxed inserts B, E and H are areas shown at higher magnification in the central panel. **B, E, H:** Iba1 immunolabeled cells (red) in the SV and SL (white arrows) are more densely packed and overall, more intensely stained in the NES control (B) than in the ES condition (E, H). Iba1 immunolabeled activated macrophage/microglia are seen packed in a distinct "palisade" pattern at the border between the SV and SL in NES control (B). Such "microglial palisade" is seen more attenuated in the ES condition in both cochleae, ipsilateral (E, ES-IPSI) and contralateral (H, ES-CONTRA) to the side of the cortical electrical stimulation. Immunolabeled cellular processes in the lateral wall look longer and thinner in the ES condition (E, H). **C, F, I:** Iba1 immunolabeled cell processes (red) are seen among spiral ganglion neurons counterstained with Phalloidin (green). No differences are seen in their distribution and morphology between NES (C) and ES (F, I) conditions. Blue staining corresponds to DAPI-counterstained nuclei. Abbreviations: SV, stria vascularis; SL, spiral ligament. Scale bars: 50μm in G; 20μm in H and I.

immunostaining levels in MOC endings underneath OHCs has been shown using a similar approach of cortical electrical stimulation after noise exposure (Diaz et al., 2021). It is also relevant that the expression of nicotinic Ach receptor subunits alpha9/10 which mediate cholinergic neurotransmission at MOC efferent synapses with OHCs depends on the integrity of the AC (Lamas et al., 2017) and by extension of descending auditory projections originating from the cortex.

In sum, the reported results predict that relatively prolonged electrical stimulation of the AC during aging promotes survival, potentiates the activity, or both, of aged VNTB neurons suggesting that preservation of the MOC system may participate in delaying ARHL. Whereas unraveling specific mechanisms awaits further experimental analysis, this is the first report supporting effects of electrical stimulation of the AC during aging in neurons originating the OC efferent system.

Secondly, we tested whether the effects of electrical stimulation of the AC, after being "relayed" at least on MOC neurons, propagate down to the aging cochlea, the end target of OC efferent projections. Against the backdrop of aging mechanisms (López-Otín et al., 2023), cochlear aging and associated ARHL recapitulate the multifaceted series of events that characterize the aging process and age-related pathologies (Melgar-Rojas et al., 2015; Keithley, 2020; Wang and Puel, 2020). An account of the sequence of such cochlear aging processes and mechanisms

is out of the scope of this discussion, and details have been reviewed elsewhere (Keithley, 2020; Wang and Puel, 2020). Suffice to say, for the aims of the present work, that we focused on histological and cyto-chemical markers which may be indicative of changes triggered by cortical electrical stimulation on such cochlear aging process.

4.2. Stria vascularis: reduced dystrophy

One of such cochlear aging processes involves degenerative damage to the lateral wall, including the SV and associated spiral ligament (SL). Since originally proposed by Schuknecht (Schuknecht and Gacek, 1993) dystrophic degeneration of the SV has emerged as a central component in the pathogenesis of ARHL (Fetoni et al., 2011; Melgar-Rojas et al., 2015; Ohlemiller and Frisina, 2008; Wang and Puel, 2020; Yamasoba et al., 2013). Age-related degeneration of the SV has been reported, particularly in rodents (Ding et al., 2018; Fuentes-Santamaría et al., 2022; Lang et al., 2023; Mannström et al., 2013; Spicer and Schulte, 2002) and primates, including humans (Suzuki et al., 2006). Here we show that after two weeks of multi-session cortical electrical stimulation in aged Wistar rats, the SV in cochleae from ES animals was around 15% thicker than the SV of control NES cochleae. In addition, the micro-architecture of the SV was better preserved in cochleae from rats in the
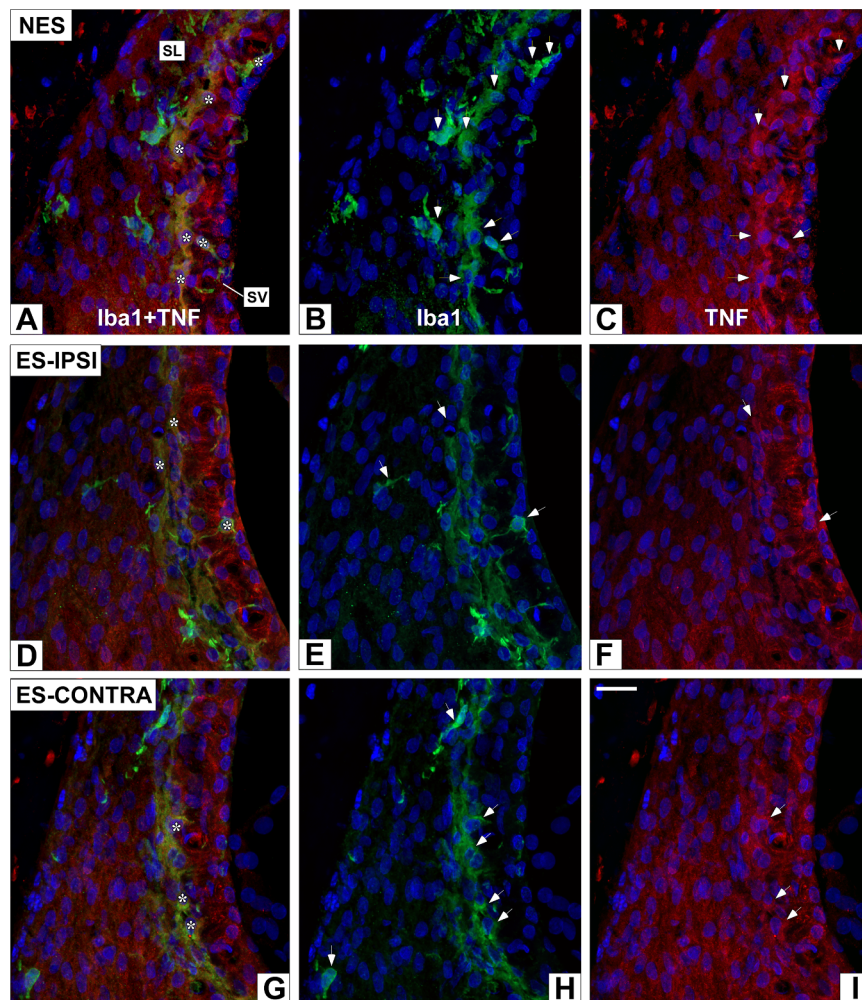
Fig. 6. TNFα and Iba1 in the stria vascularis and spiral ligament after cortical electrical stimulation during aging
A, B, C: Laser confocal scanning photomicrographs of the stria vascularis (SV) and adjacent spiral ligament (SL) from cochlear sections immunostained for Iba1 (green) and TNFα (red) from a sham implanted, non-stimulated (NES) 18-month-old rat. A is a merged image to show co-localization patterns of Iba1 and TNFα. **D-I:** Images from an old rat of the same age, after two weeks of cortical electrical stimulation (ES), corresponding respectively to the SV of the cochlea ipsilateral (ES-IPSI. D, E, F) or contralateral (ES-CONTRA. G, H, I) to the electrically stimulated side. D and G show co-localization of the Iba1 and TNFα. In the NES rat, abundant Iba1 immunolabeled activated microglia populate the SV and adjacent SL. Immunolabeled cells have thick, heterogeneous cytoplasmic extensions (white arrows in B). In contrast in the ES rat, Iba1 immunolabeling is less intense, and immunolabeled cells have thinner and longer cytoplasmic prolongations (white arrows in E and H) characteristic of less active or resting microglia. In the NES rat the overall immunolabeling intensity for TNFα in the lateral wall is higher than in the ES rat, both ipsi- and contralateral to the stimulation side (C, F and I, same conditions across immunocytochemistry runs). Activated macrophage/microglia also are immunolabeled for TNFα (white arrows in C, F and I). Co-localization of Iba 1 and TNFα is more visible in the NES control than in the ES condition (asterisks in A, D and G), suggesting down-regulation of age-related inflammation in the lateral wall after cortical electrical stimulation. Scale bar in I: 20μm.

ES group, with a discernible three cell-layered structure, characterized by more regular nuclear distribution and more homogeneous cytoplasmic definition, as well as fewer and smaller gaps between adjacent cells and tighter intercellular compartments than in the SV of the NES animal group. Altogether, these observations support that descending activation after electrical stimulation of the AC reaches the peripheral auditory receptor, improving the trophic maintenance of the SV during cochlear aging (Spicer and Schulte, 2002; Mansström et al., 2013; Ding et al. 2018; Fuentes-Santamaría et al., 2022). Such microstructural protection from age-related damage to the SV might be functionally reflected in a reversion of the age-related reduction of the endocochlear potential (Ohlemiller et al., 2006), essential to drive the activity of OHCs and hence cochlear amplification. Therefore, diminished age-related degeneration of the SV may be a key contributor to the effect of cortical electrical stimulation in reducing threshold elevation during aging, as reported by Fernández del Campo and co-workers (2024). However, thickness variations in the SV, although still likely to reflect the trophic status of the lateral wall (Suzuki et al., 2006), have been

challenged as direct markers of loss of hearing sensitivity in ARHL (Engle et al., 2013; Lang et al., 2023). Additional markers must be explored to further understand the effects of cortical electrical stimulation on cochlear function in aging.

4.3. Reduced inflammatory markers in the stria vascularis and spiral ligament

In this regard, another hallmark of cochlear aging is linked to the notion of dysregulated inflammation in the aging process and pathologies associated with aging (Franceschi and Campisi, 2014; López-Otín et al., 2023). The origins of progressively altered regulation of inflammatory mechanisms during aging are multiple. Details are, however, unknown (López-Otín et al., 2023). Regardless this gap in knowledge, it is increasingly clear that one central characteristic of aging is a lingering, chronic state of "low grade" inflammation, dubbed with the highly descriptive term of "inflammaging" (Franceschi and Campisi, 2014), which is damaging for tissues and organs (López-Otín 2023).
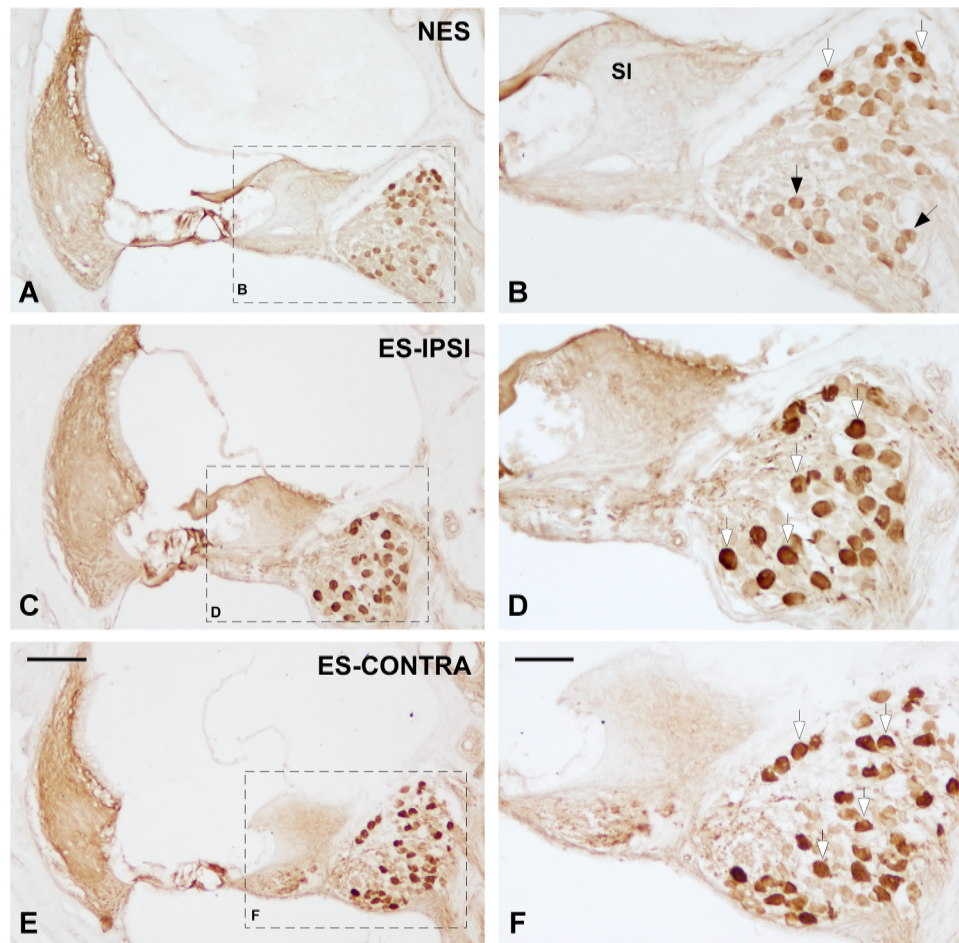
Fig. 7. Calretininin immunolabeling in the spiral ganglion after electrical stimulation of the auditory cortex during aging

A, C, E: Low magnification photomicrographs of cochlear sections immunostained with immunoperoxidase for the localization of calretinin in a sham implanted, non-stimulated (NES) 18-month-old rat (A) and in a rat of the same age after two weeks of cortical electrical stimulation (ES) in the cochlea ipsilateral (C, ES-IPSI) and contralateral (E, ES-CONTRA) to the stimulated auditory cortex. Labeled inserts in A, C and E with contours of Rosenthal's canal is shown at higher magnification in photomicrographs B, D and F. Notice immunolabeling intensity for calretinin is higher in the spiral ganglion of ES-IPSI (C) and ES-CONTRA (E) than in the NES rat (A). **B, D, F:** Higher magnification detail of calretinin immunolabeling in spiral ganglion neurons shown in inserts B, D, F. Increased calretinin immunolabeling is visible in spiral ganglion neurons from ES rats (examples highlighted with white arrows) both in the ipsilateral (D) and contralateral sides (F) of the electrically stimulated cortex, relative to spiral ganglion neurons in NES animals (black arrows). Sl: spiral limbus. Scale bars: 100μm in E; 50μm in F.

"Inflammaging" also is emerging as a key process in cochlear aging leading to ARHL (Fuentes-Santamaría et al., 2022; Lang et al., 2023; Menardo et al., 2012; Parekh and Kaur, 2023; Seicol et al., 2022; Watson et al., 2017). The lateral wall including the SV seems to play a central role in the initiation and progression of this process (Fuentes Santamaría et al., 2022; Lang et al., 2023). We have previously found significantly increased levels of immunostaining for the pro-inflammatory cytokine IL1β in the SV during aging in the Wistar rat (Fuentes Santamaría et al., 2022). TNFα, another pro-inflammatory cytokine which has been shown to be involved in the progression of noise-induced hearing loss and accelerated ARHL. (Fuentes-Santamaría et al., 2022, 2017), also increases its expression in the cochlea during aging (Lyu et al., 2020; Wu et al., 2022). Therefore, these cytokines are regarded as markers of age-related chronic inflammation (Franceschi and Campisi, 2014), including cochlear aging and associated ARHL, which is particularly evident in the lateral wall, including the SV (Watson et al., 2017). We show that after long-term electrical stimulation of the AC during aging, there are visible changes in TNFα immunolabeling in the SV and underlying SL. Such changes in immunostaining suggest modulation of age-related inflammation in the cochlea induced by cortical electrical stimulation. This is further supported by changes both in the immunolabeling pattern of Iba1, a marker of macrophage/microglia activated during the cellular transformation and migration events of inflammation (Ohsawa et al., 2004), and in the morphology of Iba1- immunolabeled cells. In the lateral wall of ES rats, including the SV and SL, Iba1-immunolabeled macrophages had a comparatively slenderer morphology, with thinner and longer processes than their NES counterparts. Iba1 immunolabeled cells look "chubbier", with thicker and shorter cytoplasmic prolongations. The latter morphology is associated with activated macrophage/microglia participating in ongoing inflammatory/immune responses, whereas the former denotes cells in resting, or comparatively inactive, cell pools (Benarroch, 2013). Also, Iba1 and TNFα immunoreactivities very often co-localize (Fuentes-Santamaria et al., 2022). In our experimental series, co-localization of Iba1 with TNFα showed diminished intensity in the lateral wall of ES rats relative to NES rats, particularly in macrophage/microglia at the border between the SV and SL. Because activated microglia are an important source of TNFα (Clausen et al., 2008), this may be an indication of down-regulation of "inflammaging" in the cochlea by cortical electrical stimulation. These findings gain additional interest in view of recent elegant evidence supporting that the density of activated macrophage/microglia in the SV is a reliable marker and predictor of the initiation and progression of degraded hearing sensitivity in ARHL (Lang et al., 2023).
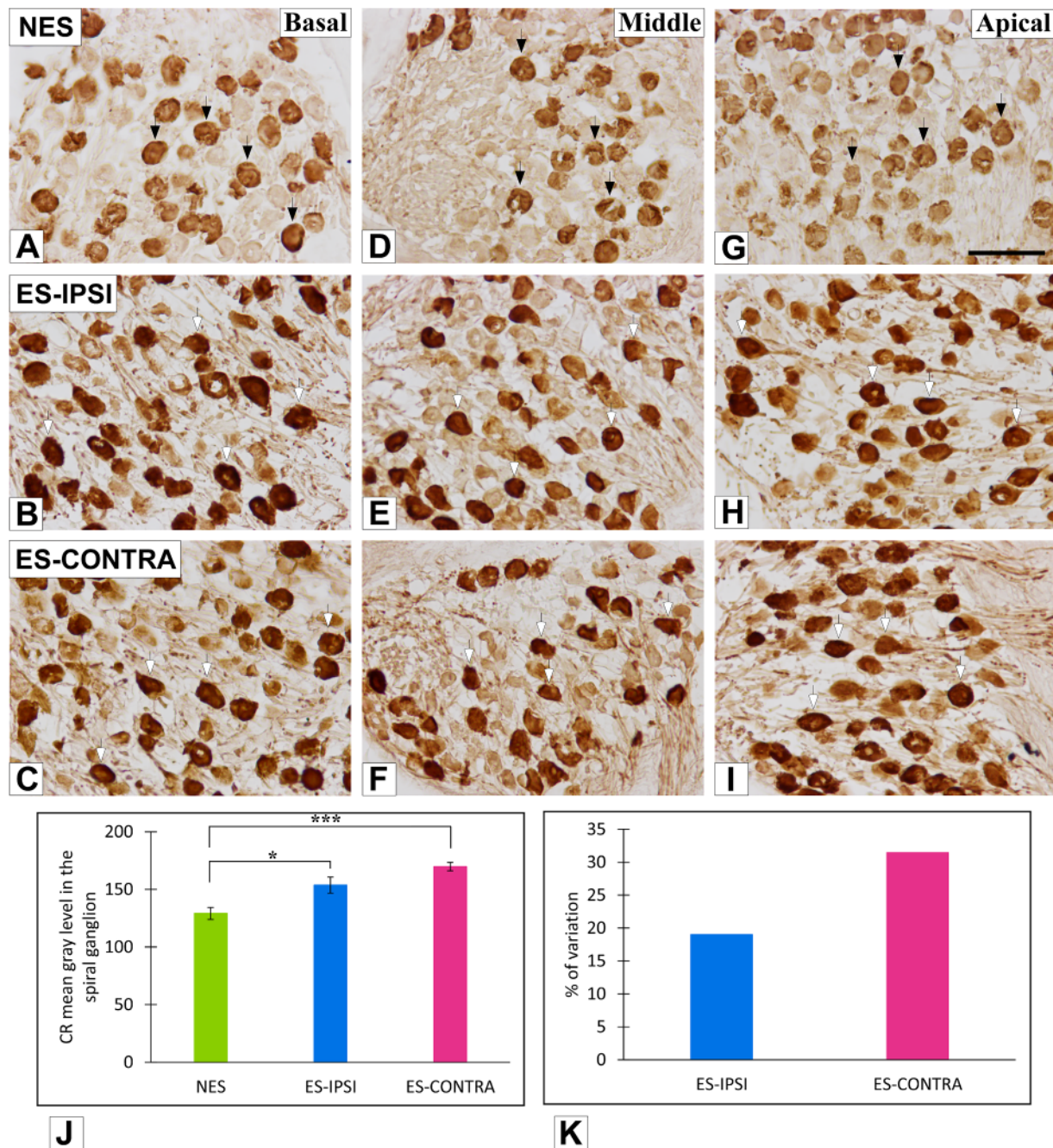
Fig. 8. Details of changes in calretinin immunolabeling in spiral ganglion neurons after cortical stimulation during aging
A-I: Photomicrographs from sections of the spiral ganglion immunostained with immunoperoxidase for the localization of calretinin in a sham implanted, non-stimulated (NES) 18-month-old rat (A, basal turn, D, middle turn, and G apical turn) and in a rat of the same age after two weeks of cortical electrical stimulation (ES) in the cochlea ipsilateral (ES-IPSI. B, basal turn, E, middle turn and H, apical turn) and contralateral (ES-CONTRA. C, basal turn, F, middle turn, I, apical turn) to the stimulated auditory cortex. More intense immunolabeling for calretinin is detectable in spiral ganglion neuron cell bodies from the ES (B, C, E, F, H, I) than from the NES rat (A, D, G). Increased calretinin immunolabeling after cortical electrical stimulation is seen in spiral ganglion neuron cell bodies across all cochlear turns. **J:** Bar graph showing mean gray level of calretinin immunolabeling in spiral ganglion neuron cell bodies from NES and ES rats. A significant increase in immunolabeling intensity is found in spiral ganglion neuron cell bodies in ES rats, both in ES-IPSI and ES-CONTRA. **K:** Bar graph showing percentage of variation of calretinin immunolabeling between mean gray levels in spiral ganglion neuron cell bodies from ES-IPSI and ES-CONTRA. Notice a greater effect of cortical electrical stimulation on calretinin immunoreactivity levels on spiral ganglion neuron cell bodies in the side contralateral to the stimulated cortex. Comparisons among the different groups were performed using two-way ANOVA ($F_{(2, 39)} = 12.89$) and Scheffé post hoc analysis was used for comparisons among groups. Significance levels (α) and power (β) were set to 0.05 and 95%, respectively. *$p < 0.05$; ***$p < 0.001$. Scale bar: 50μm in G.

At this stage, it is only possible to speculate on mechanisms mediating the observed effects of cortical electrical stimulation on age-related dystrophy and inflammatory dysregulation in the SV and SL. Damage to OC efferents accelerates age-related loss of hearing sensitivity suggesting that integrity of these inputs to the cochlea is necessary for long-term maintenance of cochlear function (Liberman et al., 2014). However, it is unclear whether this effect depends only on cholinergic neurotransmission on OHCs (Lauer, 2017). On the other hand, there is evidence of modulation of cochlear activity and auditory nerve responses after cortical stimulation (reviewed in Terreros and Delano,

2015). In this context, normal expression of cholinergic receptor subunits, involved in MOC neurotransmission on OHCs, and prestin transcripts involved in OHC motility and cochlear micromechanics, require integrity of the AC (Lamas et al., 2017, 2015) further supporting that cochlear activity is influenced by projections descending from the AC. Activity gain in the aging cochlea after cortical electrical stimulation may promote recovery of trophic interactions among cell populations leading to reduced damage to the SV and its microcirculation, which may downregulate cochlear inflammation (Fuentes-Santamaría et al., 2022). Clearly, more work is needed to unravel mechanisms in detail.

4.5. Increased calretinin in spiral ganglion neurons

Finally, we report increased calretinin immunoreactivity in SG neuron cell bodies after the stimulation protocol, supporting that primary auditory neurons react to cortical electrical stimulation. Calretinin is a Ca^{++}-binding protein, involved in regulation of neuronal excitability by providing fast intracellular Ca^{++} buffering (Camp and Wijesinghe, 2009). SG neurons express different combinations of calretinin and calbindin, another Ca^{++}-binding protein (Fischer et al., 2019; Liu and Davis, 2014; Shrestha et al., 2018; Wang et al., 2023). It has been proposed that its expression levels depend on cochlear activity (Alvarado et al., 2016; Shrestha et al., 2018). Also changes in immunolabeling intensity of Ca^{++}-binding proteins have been reported in peripheral and central auditory neurons in ARHL, and these may be linked at least in part to adaptive or compensatory mechanisms for progressively degraded hearing activity (Fischer et al., 2019; Idrizbegovic et al., 2004; Ouda et al., 2012; Wang et al., 2023). Insofar increased calretinin levels may be construed as part of excitability modulation mechanisms in SG neurons, increased calretinin immunoreactivity shown in the ES group, evokes compensatory adaptation of primary auditory neurons to cortical electrical stimulation during aging. We have previously shown that integrity of the AC is needed for normal expression in the cochlea of gene transcripts coding for ionotropic glutamate receptor subunits in SG neurons, involved in excitatory neurotransmission at the IHC-SG neuron synapse (Lamas et al., 2017). Thus, SG neuron excitability seems to be regulated by corticofugal pathways, which may be one foundation of previously reported descending modulation of cochlear responses (Lesicko and Llano, 2017; Terreros and Delano, 2015). Our findings, however, do not allow to draw conclusions about how electrical stimuli delivered to the surface of the AC are channeled to modify excitability in aged SG neurons. In this regard, it is known that the LOC system modulates activity on primary auditory neurons (Groff and Liberman, 2003; Le Prell et al., 2003) and that firing of LOC neurons is induced by projections descending from the auditory midbrain (Groff and Liberman, 2003). These in turn may be activated by corticofugal projections (Terreros and Delano, 2015), although they have not been characterized so far. In addition, one limitation of our level of analysis based on quantitative ChAT immunolabeling on brainstem neurons is that it only allowed to recognize effects of cortical electrical stimulation on MOC neurons in VNTB, but not in LOC neurons, for which unambiguous identification was not possible. To what extent both MOC and LOC systems are involved in mediating the effects of cortical electrical stimulation on the aging cochlea and its specific contributions must be addressed in the future.

5. Conclusions

Long-term electrical stimulation of the AC may result in activation of descending pathways, propagating down to the cochlea. Preservation of ChAT immunolabeling in MOC neurons in the VNTB supports effects of cortical electrical stimulation on cochlear aging mediated through activation of the efferent system. Structural preservation of the SV and reduced immunolabeling for inflammatory markers along with possible modulation of activity in aged SG neurons shown after AC stimulation, determines an effective delay in cochlear aging. Both set of results

together, as well as previous evidence of the otoprotective effect of the efferent system in cochlear function, supports that MOC preservation through corticofugal electrical activation at the level of the AC may be a good approach for ameliorating the impact of presbycusis.

Author statement

The authors are aware of this submission and have authorized their inclusion as co-authors in the manuscript.

CRediT authorship contribution statement

V. Fuentes-Santamaría: Conceptualization, Methodology, Formal analysis, Investigation, Writing – review & editing. **Z. Benítez-Maicán:** Methodology, Formal analysis, Investigation. **J.C. Alvarado:** Conceptualization, Methodology, Formal analysis, Resources, Writing – review & editing, Funding acquisition. **I.S. Fernández del Campo:** Methodology, Formal analysis, Investigation. **M.C. Gabaldón-Ull:** Methodology, Investigation. **M.A. Merchán:** Conceptualization, Methodology, Formal analysis, Resources, Writing – original draft, Writing – review & editing, Supervision, Project administration, Funding acquisition. **J.M. Juiz:** Conceptualization, Methodology, Formal analysis, Resources, Writing – original draft, Writing – review & editing, Supervision, Project administration, Funding acquisition.

Declaration of competing interest

The authors declare that the research was conducted in the absence of any commercial or financial relationships that could be construed as a potential conflict of interest.

Data availability

Data will be made available on request.

References

Abdala, C., Dhar, S., Ahmadi, M., Luo, P., 2014. Aging of the medial olivocochlear reflex and associations with speech perception. J. Acoust. Soc. Am. 135, 754. https://doi.org/10.1121/1.4861841.

Altschuler, R.A., Hoffman, D.W., Wenthold, R.J., 1986. Neurotransmitters of the cochlea and cochlear nucleus: immunocytochemical evidence. Am. J. Otolaryngol. 7, 100–106. https://doi.org/10.1016/S0196-0709(86)80038-2.

Alvarado, J.C., Fuentes-Santamaría, V., Gabaldón-Ull, M.C., Blanco, J.L., Juiz, J.M., 2014. Wistar rats: a forgotten model of age-related hearing loss. Front Aging Neurosci 6, 29. https://doi.org/10.3389/fnagi.2014.00029.

Alvarado, J.C., Fuentes-Santamaría, V., Gabaldón-Ull, M.C., Jareño-Flores, T., Miller, J.M., Juiz, J.M., 2016. Noise-Induced "Toughening" Effect in Wistar Rats: Enhanced Auditory Brainstem Responses Are Related to Calretinin and Nitric Oxide Synthase Upregulation. Front. Neuroanat. 10 https://doi.org/10.3389/fnana.2016.00019.

Asilador, A., Llano, D.A., 2021. Top-Down Inference in the Auditory System: Potential Roles for Corticofugal Projections. Front. Neural Circuits 14. https://doi.org/10.3389/FNCIR.2020.615259.

Benarroch, E.E., 2013. Microglia: Multiple roles in surveillance, circuit shaping, and response to injury. Neurology 81, 1079–1088. https://doi.org/10.1212/WNL.0B013E3182A4A577.

Blanchet, C., Eróstegui, C., Sugasawa, M., Dulon, D., 1996. Acetylcholine-induced potassium current of guinea pig outer hair cells: its dependence on a calcium influx through nicotinic-like receptors. J. Neurosci. 16, 2574–2584. https://doi.org/10.1523/JNEUROSCI.16-08-02574.1996.

Boero, L.E., Castagna, V.C., Terreros, G., Moglie, M.J., Silva, S., Maass, J.C., Fuchs, P.A., Delano, P.H., Elgoyhen, A.B., Gómez-Casati, M.E., 2020. Preventing presbycusis in mice with enhanced medial olivocochlear feedback. Proc. Natl. Acad. Sci. U. S. A. 117, 11811–11819. https://doi.org/10.1073/PNAS.2000760117/SUPPL_FILE/PNAS.2000760117.SAPP.PDF.

Camp, A.J., Wijesinghe, R., 2009. Calretinin: Modulator of neuronal excitability. Int. J. Biochem. Cell Biol. 41, 2118–2121. https://doi.org/10.1016/J.BIOCEL.2009.05.007.

Carbajal, G.V., Malmierca, M.S., 2018. The Neuronal Basis of Predictive Coding Along the Auditory Pathway: From the Subcortical Roots to Cortical Deviance Detection. Trends Hear 22. https://doi.org/10.1177/2331216518784822.

Clausen, B.H., Lambertsen, K.L., Babcock, A.A., Holm, T.H., Dagnaes-Hansen, F., Finsen, B., 2008. Interleukin-1 beta and tumor necrosis factor-alpha are expressed by different subsets of microglia and macrophages after ischemic stroke in mice. J. Neuroinflammation 5, 1–18. https://doi.org/10.1186/1742-2094-5-46/FIGURES/7.

Colmenárez-Raga, A.C., Díaz, I., Pernia, M., Pérez-González, D., Delgado-García, J.M., Carro, J., Plaza, I., Merchán, M.A., 2019. Reversible Functional Changes Evoked by Anodal Epidural Direct Current Electrical Stimulation of the Rat Auditory Cortex. Front Neurosci 13, 356. https://doi.org/10.3389/fnins.2019.00356.

De Ridder, D., Adhia, D., Langguth, B., 2021. Tinnitus and Brain Stimulation. Curr. Top. Behav. Neurosci. 51, 249–293. https://doi.org/10.1007/7854_2021_219.

Díaz, I., Colmenárez-Raga, A.C., Pérez-González, D., Carmona, V.G., Plaza Lopez, I., Merchán, M.A., 2021. Effects of Multisession Anodal Electrical Stimulation of the Auditory Cortex on Temporary Noise-Induced Hearing Loss in the Rat. Front. Neurosci. 15 https://doi.org/10.3389/FNINS.2021.642047.

Ding, B., Walton, J.P., Zhu, X., Frisina, R.D., 2018. Age-related changes in Na, K-ATPase expression, subunit isoform selection and assembly in the stria vascularis lateral wall of mouse cochlea. Hear. Res. 367, 59. https://doi.org/10.1016/J.HEARES.2018.07.006.

Elgoyhen, A.B., Katz, E., 2012. The efferent medial olivocochlear-hair cell synapse. J. Physiol. Paris 106, 47–56. https://doi.org/10.1016/J.JPHYSPARIS.2011.06.001.

Elgueda, D., Delano, P.H., 2020. Corticofugal modulation of audition. Curr. Opin. Physiol. 18, 73–78. https://doi.org/10.1016/J.COPHYS.2020.08.016.

Engle, J.R., Tinling, S., Recanzone, G.H., 2013. Age-Related Hearing Loss in Rhesus Monkeys Is Correlated with Cochlear Histopathologies. PLoS One 8. https://doi.org/10.1371/JOURNAL.PONE.0055092.

Fernández del Campo, I.S., Carmona-Barón, V.G., Diaz, I., Plaza, I., Alvarado, J.C., Merchán, M.A, 2024. Multisession anodal epidural direct current stimulation of the auditory cortex delays the progression of presbycusis in the Wistar rat. Hearing Res in this issue.

Fetoni, A.R., Picciotti, P.M., Paludetti, G., Troiani, D., 2011. Pathogenesis of presbycusis in animal models: a review. Exp. Gerontol. 46, 413–425. https://doi.org/10.1016/J.EXGER.2010.12.003.

Fischer, N., Johnson Chacko, L., Majerus, A., Potrusil, T., Riechelmann, H., Schmutzhard, J., Schrott-Fischer, A., Glueckert, R., 2019. Age-dependent calcium-binding protein expression in the spiral ganglion and hearing performance of c57bl/6j and 129/svj mice. ORL 81, 138–154. https://doi.org/10.1159/000499472.

Franceschi, C., Campisi, J., 2014. Chronic Inflammation (Inflammaging) and Its Potential Contribution to Age-Associated Diseases. Biol. Sci. Cite J. as J Gerontol A Biol Sci Med Sci 69. https://doi.org/10.1093/gerona/glu057.

Fuchs, P.A., Lauer, A.M., 2019. Efferent Inhibition of the Cochlea. Cold Spring Harb. Perspect. Med. 9 https://doi.org/10.1101/CSHPERSPECT.A033530.

Fuentes-Santamaría, V., Alvarado, J.C., Melgar-Rojas, P., Gabaldón-Ull, M.C., Miller, J. M., Juiz, J.M., 2017. The role of glia in the peripheral and central auditory system following noise overexposure: Contribution of TNF-α and IL-1β to the pathogenesis of hearing loss. Front. Neuroanat. 11 https://doi.org/10.3389/fnana.2017.00009.

Fuentes-Santamaría, V., Alvarado, J.C., Mellado, S., Melgar-Rojas, P., Gabaldón-Ull, M. C., Cabanes-Sanchis, J.J., Juiz, J.M., 2022. Age-Related Inflammation and Oxidative Stress in the Cochlea Are Exacerbated by Long-Term, Short-Duration Noise Stimulation. Front. Aging Neurosci. 14 https://doi.org/10.3389/FNAGI.2022.853320.

Fuentes-Santamaría, V., Alvarado, J.C., Rodríguez-de la Rosa, L., Juiz, J.M., Varela-Nieto, I., 2019. Neuroglial involvement in abnormal glutamate transport in the cochlear nuclei of the Igf1−/− mouse. Front. Cell. Neurosci. 13 https://doi.org/10.3389/fncel.2019.00067.

Fuentes-Santamaría, V., Alvarado, J.C., Taylor, A.R., Brunso-Bechtold, J.K., Henkel, C.K., 2005. Quantitative changes in calretinin immunostaining in the cochlear nuclei after unilateral cochlear removal in young ferrets. J. Comp. Neurol. 483, 458–475. https://doi.org/10.1002/cne.20437.

Gafoor, S.A., Uppunda, A.K., 2023. Speech Perception in Noise and Medial Olivocochlear Reflex: Effects of Age, Speech Stimulus, and Response-Related Variables. J. Assoc. Res. Otolaryngol. 24 https://doi.org/10.1007/S10162-023-00919-W.

Gil-Loyzaga, P.E., 1995. Neurotransmitters of the olivocochlear lateral efferent system: With an emphasis on dopamine. Acta Otolaryngol 115, 222–226. https://doi.org/10.3109/00016489509139296.

Groff, J.A., Liberman, M.C., 2003. Modulation of cochlear afferent response by the lateral olivocochlear system: activation via electrical stimulation of the inferior colliculus. J. Neurophysiol. 90, 3178–3200. https://doi.org/10.1152/JN.00537.2003.

Guerrieri, M., Di Mauro, R., Di Girolamo, S., Di Stadio, A., 2023. Hearing and Ageing. Subcell. Biochem. 103, 279–290. https://doi.org/10.1007/978-3-031-26576-1_12.

Guinan, J.J., Warr, W.B., Norris, B.E., 1983. Differential olivocochlear projections from lateral versus medial zones of the superior olivary complex. J. Comp. Neurol. 221, 358–370. https://doi.org/10.1002/CNE.902210310.

Hua, Y., Ding, X., Wang, H., Wang, F., Lu, Y., Neef, J., Gao, Y., Moser, T., Wu, H., 2021. Electron Microscopic Reconstruction of Neural Circuitry in the Cochlea. Cell Rep 34. https://doi.org/10.1016/J.CELREP.2020.108551.

Hyson, R.L., Rubel, E.W., 1995. Activity-dependent regulation of a ribosomal RNA epitope in the chick cochlear nucleus. Brain Res. 672, 196–204. https://doi.org/10.1016/0006-8993(94)01390-4.

Idrizbegovic, E., Bogdanovic, N., Willott, J.F., Canlon, B., 2004. Age-related increases in calcium-binding protein immunoreactivity in the cochlear nucleus of hearing impaired C57BL/6J mice. Neurobiol. Aging 25, 1085–1093. https://doi.org/10.1016/j.neurobiolaging.2003.11.004.

Kawase, T., Liberman, M.C., 1993. Antimasking effects of the olivocochlear reflex. I. Enhancement of compound action potentials to masked tones. J. Neurophysiol. 70, 2519–2532. https://doi.org/10.1152/jn.1993.70.6.2519.

Keithley, E.M., 2020. Pathology and mechanisms of cochlear aging. J. Neurosci. Res. 98, 1674. https://doi.org/10.1002/JNR.24439.

Lamas, V., Arévalo, J.C., Juiz, J.M., Merchán, M.A., 2015. Acoustic input and efferent activity regulate the expression of molecules involved in cochlear micromechanics. Front. Syst. Neurosci. 8 https://doi.org/10.3389/fnsys.2014.00253.

Lamas, V., Juiz, J.M., Merchán, M.A., 2017. Ablation of the auditory cortex results in changes in the expression of neurotransmission-related mRNAs in the cochlea. Hear. Res. 346, 71–80. https://doi.org/10.1016/J.HEARES.2017.02.011.

Lang, H., Noble, K.V., Barth, J.L., Rumschlag, J.A., Jenkins, T.R., Storm, S.L., Eckert, M. A., Dubno, J.R., Schulte, B.A., 2023. The Stria Vascularis in Mice and Humans Is an Early Site of Age-Related Cochlear Degeneration, Macrophage Dysfunction, and Inflammation. J. Neurosci. 43, 5057–5075. https://doi.org/10.1523/JNEUROSCI.2234-22.2023.

Lauer, A.M., 2017. Minimal Effects of Age and Exposure to a Noisy Environment on Hearing in Alpha9 Nicotinic Receptor Knockout Mice. Front. Neurosci. 11 https://doi.org/10.3389/FNINS.2017.00304.

Lefaucheur, J.-P., 2008. Principles of therapeutic use of transcranial and epidural cortical stimulation. 10.1016/j.clinph.2008.07.007.

Le Prell, C.G., Shore, S.E., Hughes, L.F., Bledsoe Jr., S.C., 2003. Disruption of lateral efferent pathways: functional changes in auditory evoked responses. J Assoc Res Otolaryngol 4, 276–290. https://doi.org/10.1007/s10162-002-3018-6.

Lesicko, A.M.H., Llano, D.A., 2017. Impact of peripheral hearing loss on top-down auditory processing. Hear. Res. 343, 4–13. https://doi.org/10.1016/J.HEARES.2016.05.018.

Liberman, L.D., Liberman, M.C., 2019. Cochlear Efferent Innervation Is Sparse in Humans and Decreases with Age. J. Neurosci. 39, 9560–9569. https://doi.org/10.1523/JNEUROSCI.3004-18.2019.

Liberman, M.C., Liberman, L.D., Maison, S.F., 2014. Efferent Feedback Slows Cochlear Aging. J. Neurosci. 34, 4599. https://doi.org/10.1523/JNEUROSCI.4923-13.2014.

Liu, W., Davis, R.L., 2014. Calretinin and calbindin distribution patterns specify subpopulations of type I and type II spiral ganglion neurons in postnatal murine cochlea. J. Comp. Neurol. 522, 2299–2318. https://doi.org/10.1002/cne.23535.

López-Otín, C., Blasco, M.A., Partridge, L., Serrano, M., Kroemer, G., 2023. Hallmarks of aging: An expanding universe. Cell 186, 243–278. https://doi.org/10.1016/J.CELL.2022.11.001.

Lopez-Poveda, E.A., 2018. Olivocochlear Efferents in Animals and Humans: From Anatomy to Clinical Relevance. Front. Neurol. 9 https://doi.org/10.3389/FNEUR.2018.00197.

Lyu, A.R., Kim, T.H., Park, S.J., Shin, S.A., Jeong, S.H., Yu, Y., Huh, Y.H., Je, A.R., Park, M.J., Park, Y.H., 2020. Mitochondrial Damage and Necroptosis in Aging Cochlea. Int. J. Mol. Sci. 21 https://doi.org/10.3390/IJMS21072505.

Malmierca, M., Ryugo, D., 2011. Descending Connections of Auditory Cortex to the Midbrain and Brain Stem. In: Winer, J.A., Schreiner, C.E. (Eds.), The auditory cortex. Springer, New York, pp. 189–208.

Mannström, P., Ulfhake, B., Kirkegaard, M., Ulfendahl, M., 2013. Dietary restriction reduces age-related degeneration of stria vascularis in the inner ear of the rat. Exp. Gerontol. 48, 1173–1179. https://doi.org/10.1016/J.EXGER.2013.07.004.

Marrufo-Pérez, M.I., Eustaquio-Martín, A., Lopez-Poveda, E.A., 2018. Adaptation to Noise in Human Speech Recognition Unrelated to the Medial Olivocochlear Reflex. J. Neurosci. 38, 4138. https://doi.org/10.1523/JNEUROSCI.0024-18.2018.

Melgar-Rojas, P., Alvarado, J.C., Fuentes-Santamaría, V., Juiz, J.M., 2015. Cellular Mechanisms of Age-Related Hearing Loss. In: Miller, J., Le Prell, C.G., Rybak, L. (Eds.), Free Radicals in ENT Pathology. Humana Press, pp. 305–333. https://doi.org/10.1007/978-3-319-13473-4_15.

Menardo, J., Tang, Y., Ladrech, S., Lenoir, M., Casas, F., Michel, C., Bourien, J., Ruel, J., Rebillard, G., Maurice, T., Puel, J.L., Wang, J., 2012. Oxidative stress, inflammation, and autophagic stress as the key mechanisms of premature age-related hearing loss in SAMP8 Mouse Cochlea. Antioxidants Redox Signal 16, 263–274. https://doi.org/10.1089/ars.2011.4037.

Mosilhy, E.A., Alshial, E.E., Eltaras, M.M., Rahman, M.M.A., Helmy, H.I., Elazoul, A.H., Hamdy, O., Mohammed, H.S., 2022. Non-invasive transcranial brain modulation for neurological disorders treatment: A narrative review. Life Sci 307, 120869. https://doi.org/10.1016/J.LFS.2022.120869.

Ohlemiller, K.K., Frisina, R.D., 2008. Age-Related Hearing Loss and Its Cellular and Molecular Bases. In: Schacht, J., Popper, A.N., Fay, R.R. (Eds.), Auditory Trauma Protection and Repair. Springer, New York, pp. 145–194. https://doi.org/10.1007/978-0-387-72561-1_6.

Ohlemiller, K.K., Lett, J.M., Gagnon, P.M., 2006. Cellular correlates of age-related endocochlear potential reduction in a mouse model. Hear. Res. 220, 10–26. https://doi.org/10.1016/J.HEARES.2006.06.012.

Ohsawa, K., Imai, Y., Sasaki, Y., Kohsaka, S., 2004. Microglia/macrophage-specific protein Iba1 binds to fimbrin and enhances its actin-bundling activity. J. Neurochem. 88, 844–856. https://doi.org/10.1046/J.1471-4159.2003.02213.X.

Ouda, L., Burianova, J., Syka, J., 2012. Age-related changes in calbindin and calretinin immunoreactivity in the central auditory system of the rat. Exp. Gerontol. 47, 497–506. https://doi.org/10.1016/j.exger.2012.04.003.

Parekh, S., Kaur, T., 2023. Cochlear inflammaging: cellular and molecular players of the innate and adaptive immune system in age-related hearing loss. Front. Neurol. 14 https://doi.org/10.3389/FNEUR.2023.1308823.

Patel, R., McKinnon, B.J., 2018. Hearing Loss in the Elderly. Clin. Geriatr. Med. 34, 163–174. https://doi.org/10.1016/J.CGER.2018.01.001.

Paxinos, G., Watson, C., 2005. The Rat Brain in Stereotaxic Coordinates, 5th ed. Elsevier Academic Press, Burlington, MA, ISBN 0-12-088472-0.

Peelle, J.E., Wingfield, A., 2016. The neural consequences of age-related hearing loss. Trends Neurosci 39, 486. https://doi.org/10.1016/J.TINS.2016.05.001.

Radtke-Schuller, S., Seeler, S., Grothe, B., 2015. Restricted loss of olivocochlear but not vestibular efferent neurons in the senescent gerbil (Meriones unguiculatus). Front. Aging Neurosci. 7 https://doi.org/10.3389/FNAGI.2015.00004.

Ruel, J., Wang, J., Rebillard, G., Eybalin, M., Lloyd, R., Pujol, R., Puel, J.L., 2007. Physiology, pharmacology and plasticity at the inner hair cell synaptic complex. Hear. Res. 227, 19–27. https://doi.org/10.1016/J.HEARES.2006.08.017.

Schofield, B.R., 2010. Structural organization of the descending auditory pathway. In: Palmer, A.R., Rees, A. (Eds.), The Oxford Handbook of Auditory Science. The Auditory Brain. Oxford Academics, pp. 43–64. https://doi.org/10.1093/oxfordhb/9780199233281.013.0003.

Schuknecht, H.F., Gacek, M.R., 1993. Cochlear pathology in presbycusis. Ann. Otol. Rhinol. Laryngol. 102, 1–16. https://doi.org/10.1177/00034894931020s101.

Seicol, B.J., Lin, S., Xie, R., 2022. Age-Related Hearing Loss Is Accompanied by Chronic Inflammation in the Cochlea and the Cochlear Nucleus. Front. Aging Neurosci. 14 https://doi.org/10.3389/FNAGI.2022.846804/FULL.

Shin, S.A., Lyu, A.R., Jeong, S.H., Kim, T.H., Park, M.J., Park, Y.H., 2019. Acoustic Trauma Modulates Cochlear Blood Flow and Vasoactive Factors in a Rodent Model of Noise-Induced Hearing Loss. Int. J. Mol. Sci. 20 https://doi.org/10.3390/IJMS20215316.

Shrestha, B.R., Chia, C., Wu, L., Kujawa, S.G., Liberman, M.C., Goodrich, L.V., 2018. Sensory Neuron Diversity in the Inner Ear Is Shaped by Activity. Cell 174, 1229–1246. https://doi.org/10.1016/J.CELL.2018.07.007 e17.

Spicer, S.S., Schulte, B.A., 2002. Spiral ligament pathology in quiet-aged gerbils. Hear. Res. 172, 172–185. https://doi.org/10.1016/S0378-5955(02)00581-6.

Suzuki, T., Nomoto, Y., Nakagawa, T., Kuwahata, N., Ogawa, H., Suzuki, Y., Ito, J., Omori, K., 2006. Age-Dependent Degeneration of the Stria Vascularis in Human Cochleae. Laryngoscope 116, 1846–1850. https://doi.org/10.1097/01.MLG.0000234940.33569.39.

Terreros, G., Delano, P.H., 2015. Corticofugal modulation of peripheral auditory responses. Front. Syst. Neurosci. 9 https://doi.org/10.3389/FNSYS.2015.00134.

Tu, N.C., Friedman, R.A., 2018. Age-related hearing loss: Unraveling the pieces. Laryngoscope Investig. Otolaryngol. 3, 68. https://doi.org/10.1002/LIO2.134.

Vetter, D.E., Adams, J.C., Mugnaini, E., 1991. Chemically distinct rat olivocochlear neurons. Synapse 7, 21–43. https://doi.org/10.1002/syn.890070104.

Vicencio-Jimenez, S., Weinberg, M.M., Bucci-Mansilla, G., Lauer, A.M., 2021. Olivocochlear Changes Associated With Aging Predominantly Affect the Medial Olivocochlear System. Front. Neurosci. 15 https://doi.org/10.3389/fnins.2021.704805.

Wang, J., Puel, J.L., 2020. Presbycusis: An Update on Cochlear Mechanisms and Therapies. J. Clin. Med. 9 https://doi.org/10.3390/JCM9010218.

Wang, M., Lin, S., Xie, R., 2023. Apical-basal distribution of different subtypes of spiral ganglion neurons in the cochlea and the changes during aging. PLoS One 18. https://doi.org/10.1371/journal.pone.0292676.

Watson, N., Ding, B., Zhu, X., Frisina, R.D., 2017. Chronic inflammation – inflammaging – in the ageing cochlea: A novel target for future presbycusis therapy. Ageing Res. Rev. https://doi.org/10.1016/j.arr.2017.10.002.

White, J.S., Warr, B.W., 1983. The dual origins of the olivocochlear bundle in the albino rat. J. Comp. Neurol. 219, 203–214. https://doi.org/10.1002/CNE.902190206.

Wu, T., Zhou, J., Qiu, J., Song, Y., Guo, W., Cui, L., Song, X., Sun, Y., 2022. Tumor necrosis factor-α mediated inflammation versus apoptosis in age-related hearing loss. Front. Aging Neurosci. 14, 956503 https://doi.org/10.3389/FNAGI.2022.956503.

Yamasoba, T., Lin, F.R., Someya, S., Kashio, A., Sakamoto, T., Kondo, K., 2013. Current concepts in age-related hearing loss: epidemiology and mechanistic pathways. Hear. Res. 303, 30–38. https://doi.org/10.1016/j.heares.2013.01.021.